General Disclaimer

One or more of the Following Statements may affect this Document

- This document has been reproduced from the best copy furnished by the organizational source. It is being released in the interest of making available as much information as possible.

- This document may contain data, which exceeds the sheet parameters. It was furnished in this condition by the organizational source and is the best copy available.

- This document may contain tone-on-tone or color graphs, charts and/or pictures, which have been reproduced in black and white.

- This document is paginated as submitted by the original source.

- Portions of this document are not fully legible due to the historical nature of some of the material. However, it is the best reproduction available from the original submission.

LEGAL NOTICE

This report was prepared as an account of Government sponsored work. Neither the United States, nor the Commission, nor any person acting on behalf of the Commission:

A. Makes any warranty or representation, expressed or implied, with respect to the accuracy, completeness, or usefulness of the information contained in this report, or that the use of any information, apparatus, method, or process disclosed in this report may not infringe privately owned rights; or

B. Assumes any liabilities with respect to the use of, or for damages resulting from the use of any information, apparatus, method, or process disclosed in this report.

As used in the above, "person acting on behalf of the Commission" includes any employee or contractor of the Commission, or employee of such contractor, to the extent that such employee or contractor of the Commission, or employee of such contractor prepares, disseminates, or provides access to, any information pursuant to his employment or contract with the Commission, or his employment with such contractor.

BLANK PAGE

OAK RIDGE NATIONAL LABORATORY
operated by
UNION CARBIDE CORPORATION
for the
U. S. ATOMIC ENERGY COMMISSION

ORNL - TM - 1173

COPY NO. - 41

DATE - June 23, 1965

EXPERIMENTAL SIMULATION OF LARGE, HIGH FIELD, SUPERCONDUCTING MAGNET OPERATION

W. F. Gauster, D. L. Coffey, and H. A. Ullmaier

ABSTRACT

During the first quarter of this contract a series of new sample coils with 4 to 5-in. outside diameters for tests in the 6 $\frac{1}{2}$-in., 80-kilogauss magnet were procured. Results of tests with several of these coils are reported. Preparations for experiments in a new 13-in. bore magnet facility are progressing. The extensive recent literature on the physics of type III superconductors especially as relevant to the goals of this contract is being studied. A brief digest of a selection of several important new results is presented along with some detailed new studies on similar subjects.

BLANK PAGE

ORNL-TM-1173

Experimental Simulation of Large, High Field, Superconducting Magnet Operation

First Quarterly Report Covering the Period from

March 1 to May 31, 1965

Prepared for

George C. Marshall Space Flight Center

National Aeronautics and Space Administration

(Government Order No. H-76798)

By

Thermonuclear Division

Oak Ridge National Laboratory

Oak Ridge, Tennessee

(Operated by Union Carbide Corporation, Nuclear Division)

W. F. Gauster, Project Supervisor,

D. L. Coffey and H. A. Ullmaier, Project Engineers

CONTENTS

LIST OF FIGURES

(Pages 13-34)

EXPERIMENTAL SIMULATION OF LARGE, HIGH FIELD, SUPERCONDUCTING MAGNET OPERATION

I. ABSTRACT

During the first quarter of this contract a series of new sample coils with 4 to 5-in. outside diameters for tests in the $6\frac{1}{2}$-in., 80-kilogauss magnet were procured. Results of tests with several of these coils are reported. Preparations for experiments in a new 13-in. bore magnet facility are progressing. The extensive recent literature on the physics of type III superconductors especially as relevant to the goals of this contract is being studied. A brief digest of a selection of several important new results is presented along with some detailed new studies on similar subjects.

II. SAMPLE COIL TESTS

We will continue to employ the "Large Diameter-Small Cross Section Sample Coil" technique to study various coil winding materials and different coil designs. Additional sample coils with 4 to 5-in. outside diameter have been procured for our experiments in the $6\frac{1}{2}$-in. bore, 80-kilogauss magnet. These sample coils are of very different designs and winding materials. Details of the available sample coils are given in Table 1.

A. Coil 10.6A I_c-H_c Tests

One of the coils (10.6A of Table 1)* wound by the Linde Division of Union Carbide Corporation has been tested in both persistent and externally energized modes. In the conventional mode, with an external current source, quench data were found to be generally in agreement with our previous measurements (Fig. 1). As before (compare Fig. 9 of the previous report, ORNL-TM-1083), regions of maximum degradation occur with externally applied fields of -8 and +5 kilogauss, and a sharp peak in critical current is found in the vicinity of zero field. Data scatter in these coils has been noticeably more severe than in other epoxy impregnated coils we have tested.

---

*See page 12.

This might be a result of the input lead design used in this case, since the mechanical support of the input leads seems to be not entirely sufficient.

B. Coil 10.6A Persistent Mode Tests

By closing the persistent mode switch in zero field at 4.2°K and then slowly increasing the externally applied field a measurement of the I_c-H_c curve is possible. In our experiment a Siemens SBV552 Hall probe was located on the central plane of the coil in a mechanism which allowed positioning the probe either on axis or near the coil surface. With the coil open and not energized, the probe was first calibrated from 0 to 70 kilogauss (Fig. 2). As expected, the Hall response above 10 kilogauss is quite nonlinear. However, measurements can be made by referring to the well reproducible calibration curve. It should be emphasized that the measured field values at the center and near the coil surface were identical. Therefore no influence of diamagnetic currents flowing in the open coil was apparent.

On increasing the external field from zero, with the coil in persistent mode, the central field H_o is seen to increase (Fig. 2a) as expected by calculation of the induced current and its resultant field.[1] Sudden transitions occur which reduce the induced current to zero and permit the complete penetration of $H_{applied}$. The self field of the coil, which is the difference $H_{applied} - H_o$, follows almost exactly the current-field relation of an externally energized coil. The different current density distribution inside the small wire cross sections is not sufficient to influence substantially the central field. Following the transition, the coil generally recovers quickly and the induced current again responds to the increasing applied field. Occasionally, however, the coil remains normal for as long as one minute.

A similar series with the probe close to the inside surface of the superconducting coil is indicated by Fig. 2b. In this position the magnitude of the field generated by the induced current is greater than that of

---

[1] C. F. Hempstead, Y. B. Kim and A. R. Strnad, J. Appl. Phys. 34, 3226 (1963).

the applied field and the resultant field decreases with increasing external field.

A plot of I_c-H_c derived from Fig. 2 and other similar tests indicates critical currents comparable to the data using externally applied currents up to about 10 kilogauss. At higher fields lower critical currents are apparent (Fig. 3). This performance is not easy to understand and further analysis is needed. It should be noted that tests of this kind have been made up to now only with this one coil and may not be typical.

C. Tests with Argonne National Laboratory Cable Coils

Coils 723, 724 and 725 of Table 1 were wound by Charles Laverick of Argonne National Laboratory. They incorporate several protective devices used in his large cable coils. Zero field tests made together with Charles Laverick in his laboratory indicated critical currents of 147, 460 and 162 amperes, respectively, at 4.2°K. Figure 4 shows the results of tests at 2.5, 4.2 and 5.0°K with coil 725. The voltage drop measured on coil 725 at 4.2°K was relatively very high. Resistance measurements at room temperature were made in order to determine the resulting resistance of the copper cladding, copper wrapping, etc. (at room temperature the currents flowing through the NbTi wires can be neglected). At 4.2°K the copper resistance might decrease to about one hundredth the room temperature value. This value is only around six times as high as the total low-temperature coil resistance. This indicates that at the points where the voltage was measured, an appreciable current component is flowing through the copper wrapping. It might even be possible that inside the coil the current outside the superconductor wires is still appreciable (relatively high resistance between NbTi core and surrounding copper).

As mentioned previously, coil number 724 performed much better in the tests without external field. It is expected that the planned experiments in our laboratory will likewise yield better results.

An examination of coil 725 in the ORNL Magnet Laboratory produced the data of Fig. 5. Sudden resistive changes in this figure and those shown in Fig. 4 are thought to be partial or complete SC-N transitions within

the cable. The coil was disappointing with respect to its low quenching currents. However, these values were not erratic and the transitions to the normal state were not violent (Fig. 6).

D. Cryostrand 7 Coil Test

A small test coil of Cryostrand 7, supplied by the General Electric Company, has been tested up to 70 kilogauss. Above 20 kilogauss it yielded a monotonically decreasing critical current with increasing field (Fig. 7). Below 20 kilogauss a region with relatively low quenching currents is found with a minimum I_c of 76 amperes at 5 kilogauss. Constant current, variable field measurments clearly show flux jumps below 20 kilogauss which may produce the degradation.

E. Future Tests

Experiments are continuing to evaluate the other 7 Linde NbZr coils, the 2 additional Argonne NbTi coils, the 2 RCA NbSn coils and the NbZr coils wound by ORNL. Other tests are being prepared to examine the internal fields of superconducting coils under various experimental conditions.

III. A NOTE ON THE PHYSICS BACKGROUND OF THE DEVELOPMENT OF LARGE SUPERCONDUCTING MAGNET COILS

W. F. Gauster and H. A. Ullmaier

A. Introduction

Recent progress in the development of superconducting magnet coils which generate high field strengths in large volumes is very encouraging. At the same time, research on the physics of superconductivity is producing a wealth of important new results which, in part, can be immediately applied to the previously mentioned technological task. In this note, a few important cross connections of this kind shall be discussed. No attempt is made to present an exhaustive review with a complete list of references. Emphasis is placed on phenomenological descriptions using simple models.

B. SC III Cylinders in Slowly Changing Longitudinal Fields

The performance of cylinders of type III superconductors in slowly changing magnetic fields can be understood to a large extent by means of simple models proposed by Heinz London, C. P. Bean, Y. B. Kim, and others. A detailed study presented in Appendix A is a part of an analysis of these models published in the Thermonuclear Division Semiannual Progress Report ORNL-3564. These models do not take into account the microscopic structure of type III superconductors as being type II superconductors with physical imperfections.[2]

Recent publications deal with the analysis of the reversible part ($\overline{AB}$ in Fig. 8) and the irreversible part ($\overline{BC}$) of the magnetization. The first is due to the flux penetration of the homogeneous, strain-free material. A mathematical treatment based on the so-called "G L A G theory" (Ginzburg - Landau - Abrikosov - Gorkov) is in an advanced state of development. The irreversible part of the magnetization is caused by the resistance of the inhomogeneous material against the free motion of flux. Flux bundles (consisting of several flux quanta) will be pinned at low-energy

---

[2] An excellent short review paper is: J. D. Livingston, "Magnetic Hysteresis and Critical Currents in the Mixed State," presented at the Conference on Type II Superconductors, held in Cleveland, April 28-29, 1964. (General Electric Research Laboratory Report No. 64-RL-3810M).

regions. When the magnetic driving force overcomes the pinning force, "flux flow" or "flux jump" occurs (critical flux gradient). The equivalent macroscopic picture deals with a critical shielding current density j_c. Several authors have attempted to calculate the irreversible magnetization of type III superconductors.[3]

As is well known, the correlation between the magnetization M and the flux density B can be expressed by:

$$B = H + 4\pi M \ . \qquad (1)$$

For a type II superconductor specimen in the form of a cylinder with small demagnetization factor, the flux density B as a function of H can be easily found by this equation. Figure 9 is self-explanatory.

In the case of a type III superconductor, the irreversible part $\overline{BC}$ (Fig. 8) of the magnetization depends on the geometrical dimensions of the sample. M and B must be replaced by the average values $\langle M \rangle$ and $\langle B \rangle$.

$$\langle B \rangle = H + 4\pi \langle M \rangle \ . \qquad (2)$$

Fig. 10 corresponds to Fig. 9.[4]

The discontinuity between the external field H and the internal flux density B shown in Fig. 9b is real. Fig. 10b, however, should be considered primarily only as an analysis of the reversible and the irreversible parts of the field strength. Specific assumptions concerning the actual B distribution in the range $\pm H_{c1}$ have been made by various authors (see, for instance, refs. (6) and (8). An experimental method for actual B measurements in small gaps of superconducting cylinders in longitudinal fields has been worked out in this laboratory. Recently, experimental results using

---

[3] See for instance: J. Silcox and R. W. Rollins, Rev. Mod. Phys. 36, 52 (1964), and H. E. Cline, C. S. Tedman, Jr., and R. M. Ross, Phys. Rev. 137, A1767 (March 15, 1965).

[4] See Fig. 6 in W. F. Gauster, "High Field Superconductors and the Development of Superconducting Magnets," presented at the German Physical Society Meeting in Düsseldorf, October 5-9, 1964 (Proceedings, page 83).

the same method have been published by another author.[5] Unfortunately, a decisive experimental investigation of the fine structure of B, which is at least theoretically very interesting, seems to be difficult.

C. Flux Jumps in Cold-Worked Nb-25% Zr Solid and Hollow Cylinders Under Adiabatic Conditions (See Appendix B)

Partial reprint from ORNL Thermonuclear Div. Semiann. Progr. Rept., April 30, 1965, funded by AEC Activity 05 04 04 01.

D. One-Dimensional Models of Current-Carrying Type III Superconductors Exposed to External Fields

In superconducting coils, transport currents must be considered. The expression "transport current" is not applied consistently. To explain our use of the term, we suppose that an electric current flows through superconducting and nonsuperconducting parts which are electrically in series. This current shall be called "transport current." Therefore, the current flowing in a closed superconducting ring (induced by a changing external field) is not a transport current.

Figure 11 represents the case of an "infinitely" extended slab of superconducting material. The external magnetic field H_{ext} is parallel to the surface; the shielding and transport currents flow perpendicularly to the magnetic field. The transport current per unit length of the slab is

$$I = \int_{x=-a}^{+a} J(x)dx \ . \qquad (3)$$

The external field H(x) goes asymptotically to the constant value H_{ext} for distances $x \gg \ell$ (Fig. 12). The surface fields H_1 and H_2 are determined by

$$H_1 = H_{ext} + kI = B(+a)$$
$$H_2 = H_{ext} - kI = B(-a) \ . \qquad (4)$$

---

[5] H. T. Coffey, "Distribution of Magnetic Fields and Currents in Cold-Worked Type II Superconductors," Westinghouse Research Memo 65-1JO-CRYOA-M1 (April 15, 1965).

The constant k is 0.5×10^{-6} if H is expressed in oersted and I in amp/cm. For slowly changing fields

$$J = f(B) \; ; \tag{5}$$

the function f(B) is determined by the model used. In the simplest case (H. London - C. P. Bean model) J is either $+J_c$, $-J_c$ or zero. Kim's model employs

$$J = \frac{\alpha}{B + B_o} \; ; \tag{6}$$

Riemersma uses

$$J = \frac{\alpha}{B} \; . \tag{7}$$

Finally, the special form

$$\frac{dH}{dx} = \frac{4\pi}{10} J \tag{8}$$

of Maxwell's equation will be considered.

Simple one-dimensional models of current-carrying type III superconductors have been described by H. Riermersma,[6] J. D. Livingston,[2] M. A. R. LeBlanc et al.,[7] and others. They allow one to determine the current density and field distributions in an infinitely long slab for any H-I (path 0, 1, 2) or I-H (path 0, 3, 2) sweep (Fig. 13). A few simple examples will be discussed here. The H. London - C. P. Bean model will be used. The fields can be conveniently expressed as multiples of the field strength H_s (Fig. 14) which is determined by the critical current density J_c and the slab thickness 2a. We normalize the transport current by dividing I by $I_o = 2aJ_c$.

First, we assume that without an external field H_s the transport current is raised from zero to $0.6\ I_o$. Therefore $H_1 = -H_2 = 0.6\ H_s$ (Fig. 15, broken line). The H_{ext} is first raised to $0.4\ H_s$ (dotted line). Finally H_{ext} is increased to $1.1\ H_s$ (solid line). The corresponding current density distributions are likewise indicated in Fig. 15. At the final stage $\langle B \rangle$ is easily found to be $0.78\ H_s$. From Eq. (2) it follows that $-4\pi \langle M \rangle = 0.32\ H_s$.

---

[6] H. Riemersma, J. Appl. Phys. 35, 1802 (1964).

[7] M. A. R. LeBlanc et al., Appl. Phys. Letters 6, 189 (1965).

Now the other sweep sequence will be considered. First, the external field H_{ext} is increased from zero to 1.1 H_s, while I = 0. In Fig. 16 the B-distribution is shown by a broken line. Then the current is first raised to 0.3 I_o(Fig. 16, dotted line). Finally, the current is increased to 0.6 I_o(solid line). Now we find $\langle B \rangle$ = 0.9 H_s. Therefore $-4\pi \langle M \rangle$ = 0.2 H_s.

By reaching the same final values of H_{ext} and I by means of different sweep sequences, substantially different flux and current density distributions (and therefore different $\langle M \rangle$ values) have been obtained. The magnetization can be experimentally determined in a simple way and thus the basic assumptions of these derivations can be checked easily. Extensive work of this kind has been done by M. A. R. LeBlanc.[7] Here we will restrict ourselves to describing briefly the magnetization behavior obtained in the following ways.

Case I: No transport current I, H_{ext} cycled (Fig. 17, curve I).

Case II: No external field H_{ext}, I cycled; $\langle M \rangle$ is always zero.

Case III: Sweep sequence I-H (curve III).

Case IV: Sweep sequence H-I. For clarity's sake, no complete magnetization cycle is shown. When raising H without transport current, the first branch of curve I is obtained. The point P_o corresponds to H_{ext} = 1.8 H_s. Now by raising the transport current I to 0.2, 0.4.....1.0 I_o, respectively, the points P_1, P_2,....P_5 are obtained. As shown previously, the magnetization decreases with increasing transport current. More complete discussions can be found in papers by LeBlanc et al.

The one-dimensional model of a type III superconductor carrying a transport current and exposed to an external field can be used to investigate the low field instability regions which are important for the occurrence of flux jumps. Physical criteria (such as the temperature criterion) must be introduced. The following section deals with the so-called annihilation instability. However, there are still other possible flux jump criteria which will be discussed at another time.

E. Annihilation Instability

M. R. Beasley et al.[8] use the concept of the annihilation instability to explain the low field performance of hard superconductors. They consider the possibility that neighboring fluxoids with opposite flux directions will annihilate mutually wherever adjacent regions within a superconductor have opposite directions of magnetic induction B. In this connection the behavior of the superconductor in the range $\pm H_{c1}$ is of interest.

In the following a few special cases will be discussed. We will employ the simplest one-dimensional model; a straight-forward representation will be used which neglects the actual value of H_{c1}.

1) The two field sweep sequences H-I and I-H are considered (Fig. 13). Previously it has been shown how to find the B and J distributions easily. If the B-distribution curve cuts the zero line once, the quenching probibility due to flux bundle annihilation is indicated in Fig. 18 by a solid line. There are also ranges in which B changes its sign twice (Fig. 18, thick solid line). It can be seen that the sweep sequence I-H is the more "dangerous" one.

Several authors investigated a somewhat more complicated sweep sequence. Before going through the above mentioned sweeps, they applied negative fields, returned to field zero and started from there with a new sweep sequence. This procedure can be modified by quenching at a negative field value.

2) The maximum negative field is small; no quenching (Fig. 19). Short additional field zones occur for small field and current values, respectively.

3) The same, however, with quenching at the maximum value of the negative field (Fig. 20). The influence of the quenching is very obvious.

4) Sweep sequence similar to (b), however, with a large negative field (Fig. 21).

---

[8] M. R. Beasley et al., Phys. Rev. 137, A1205 (1965).

5) Sweep sequence similar to (4), however, with quenching (Fig. 22). Cases (3), (4) and (5) yield identical instability zones. It must be emphasized that all these results depend, of course, largely on the values of the transport currents, external fields, critical current densities and the thickness of the slab. More detailed applications of similar considerations to experiments done with superconducting ribbons and bifilarly wound coils are reported in the previously mentioned paper by Beasley et al.[8] Short sample performance under similar conditions has been studied by B. Taquet.[9]

6) C. H. Rosner and H. W. Schadler[10] observed that Nb-25% Zr short wire tests showed appreciably "degraded" results when current and field were increased simultaneously ("coil simulation" tests). However, similar experiments with Nb_3Sn[11] yielded no differences when different sweep modes were used. Recently, several authors pointed out that copper plated Nb-25% (manufactured with modified metallurgical processes) did likewise not display degradation of the mentioned kind.

An analysis of the performance of a type III superconducting slab by means of the simple one-dimensional model can be made for simultaneous I-H sweeps. An application of the flux bundle annihilation principle to these cases does not indicate additional instabilities. There are, however, other possibilities for unstable performance, which will be discussed at another time.

---

[9] Oral communication.

[10] C. H. Rosner and H. W. Schlader, J. Appl. Phys. 34, 2107 (1964), and
[11] C. H. Rosner et al., J. Appl. Phys. 34, 2108 (1964).

Table 1. New Sample Coils at the ORNL Magnet Laboratory

Coil	Material	Protection	Wound by	ID, in.	OD, in.	Length, in.	Turns	Special Features
18.3A	0.014" Nb-25% Zr Supercon	0.0014" radial copper plating	Linde	4.125	5	0.375	429	Epoxy vacuum potted; persistent mode switches provided.
18.3B	0.014"	0.0014"	Linde	4.125	5	0.375	428	
14A	0.010"	0.0010"	Linde	4.125	5	0.375	850	
14B	0.010"	0.0010"	Linde	4.125	5	0.375	852	
10.6A	0.007"	0.0007"	Linde	4.125	5	0.375	1471	
10.6B	0.007"	0.0007"	Linde	4.125	5	0.375	1472	
7.3A	0.005"	0.0005"	Linde	4.125	5	0.375	2549	
7.3B	0.005"	0.0005"	Linde	4.125	5	0.375	2551	
1010	NbSn-RCA	Mylar-Copper-Mylar interlayer	RCA	4.25	5	1	611	
1011	NbSn-RCA	Mylar-Copper-Mylar interlayer	RCA	4.25	5	1	611	
723	NbTi (Westinghouse HI-120) 0.010"/ strand, 6 strands, one cable	0.002" radial copper plating 0.014" central copper core, cadmium dipped	Argonne	2.75	4.29	1	388	
724	2 cables as in 723, bound together	Additionally 12 copper strands 0.012" wrapped around the two cables, indium dipped	Argonne	2.75	3.29	0.5	20	
725	As in 723	0.002" radial copper plating 0.014" copper core indium dipped	Argonne	2.75	3.69	0.5	56	
6032B	NbSn (Cryostrand 7)	None	G.E.	0.375	0.41	0.45	104	
5B	0.010" Nb-25% Zr Supercon	0.001" radial copper plating 0.003" shorted copper sheet interlayer	ORNL	2.225	3.75	0.75	1700	
1C	0.010" Nb-25% Zr Supercon	0.001" radial copper plating	ORNL	4.25	5	0.375	590	

ORNL DWG. 65-6939

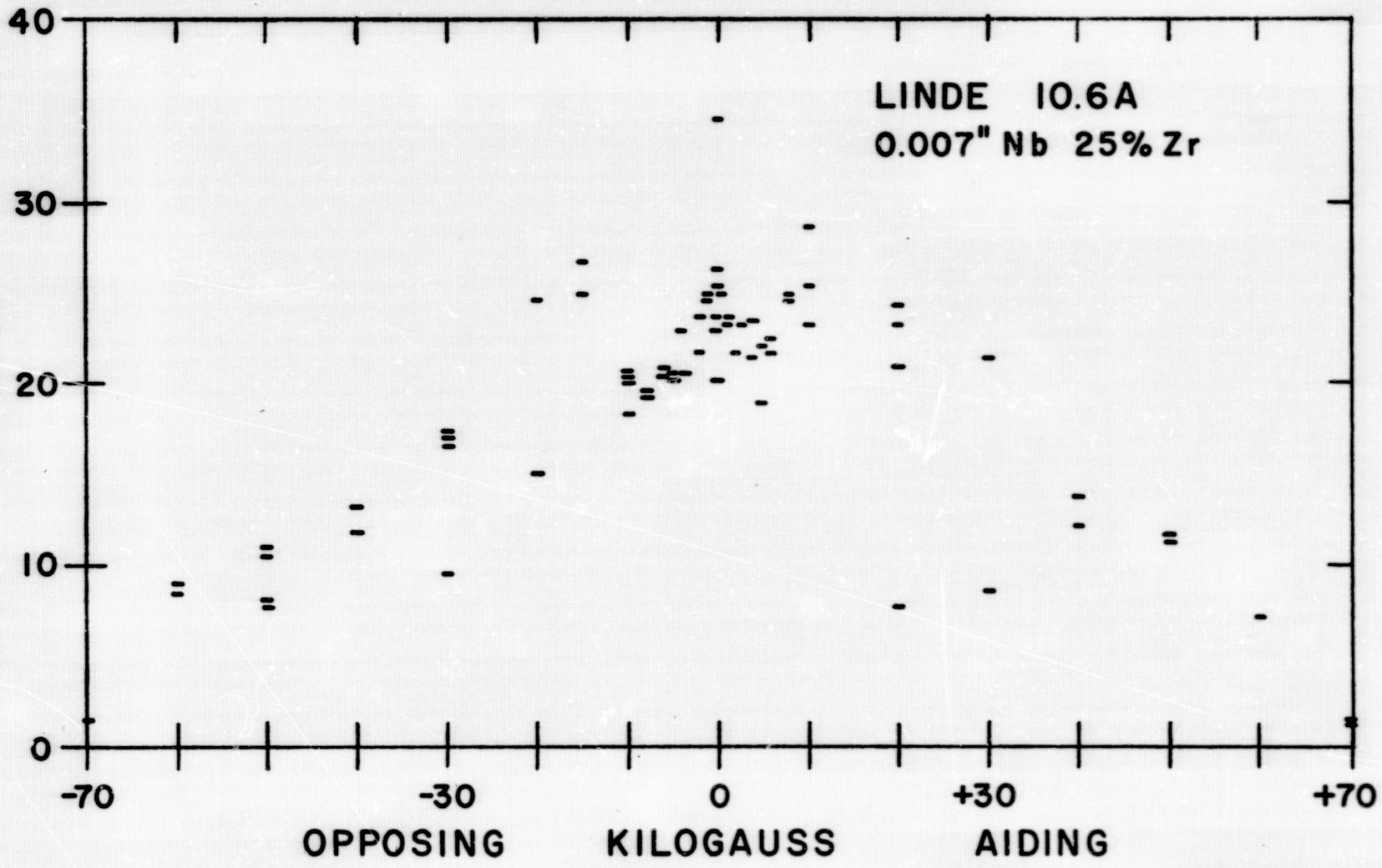

Fig. 1

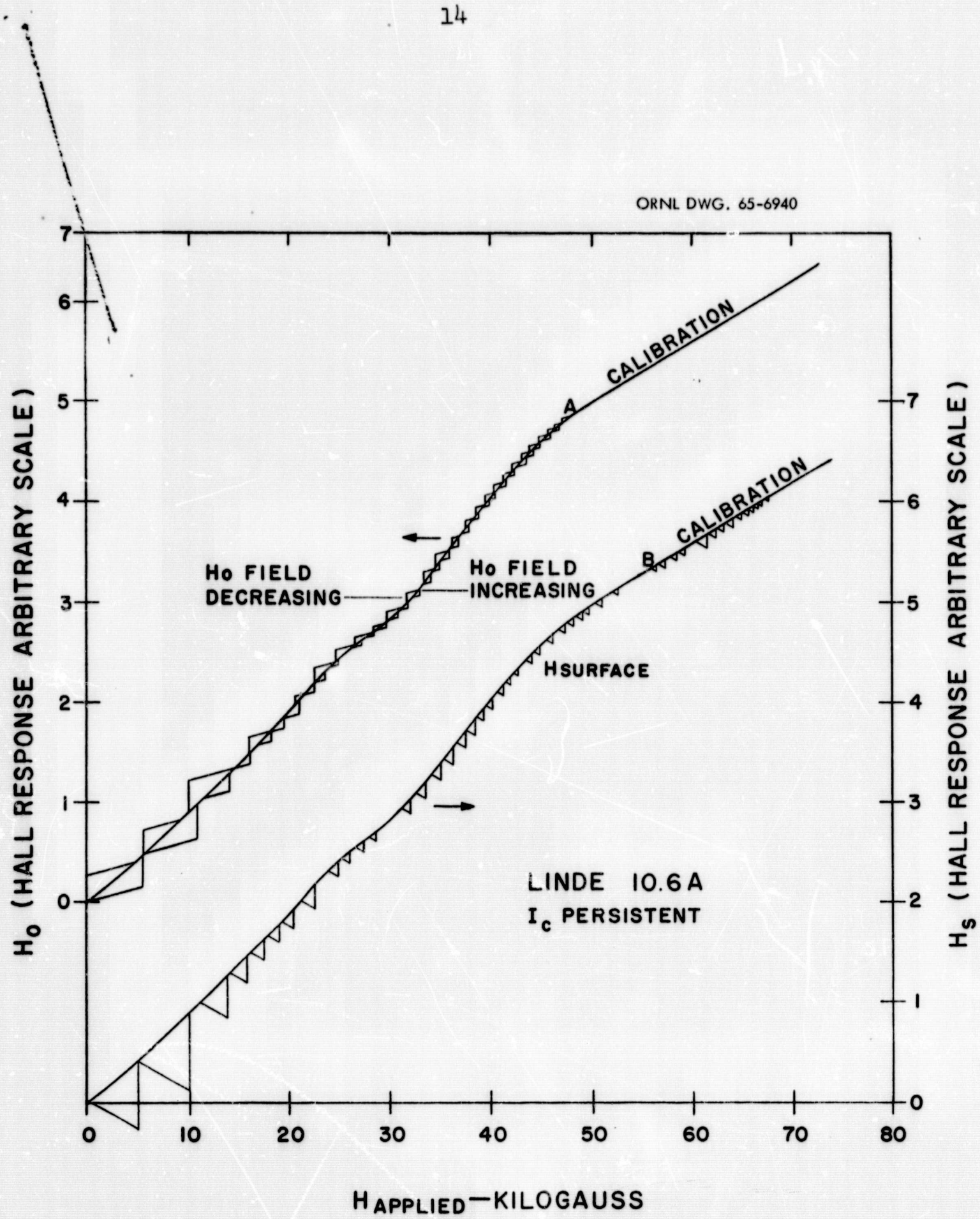
ORNL DWG. 65-6940
A CALIBRATION
B CALIBRATION
Ho FIELD DECREASING
Ho FIELD INCREASING
HSURFACE
LINDE 10.6 A
Ic PERSISTENT
Ho (HALL RESPONSE ARBITRARY SCALE)
Hs (HALL RESPONSE ARBITRARY SCALE)
HAPPLIED—KILOGAUSS
0
10
20
30
40
50
60
70
80
1
2
3
4
5
6
7

Fig. 2

ORNL DWG. 65-6941

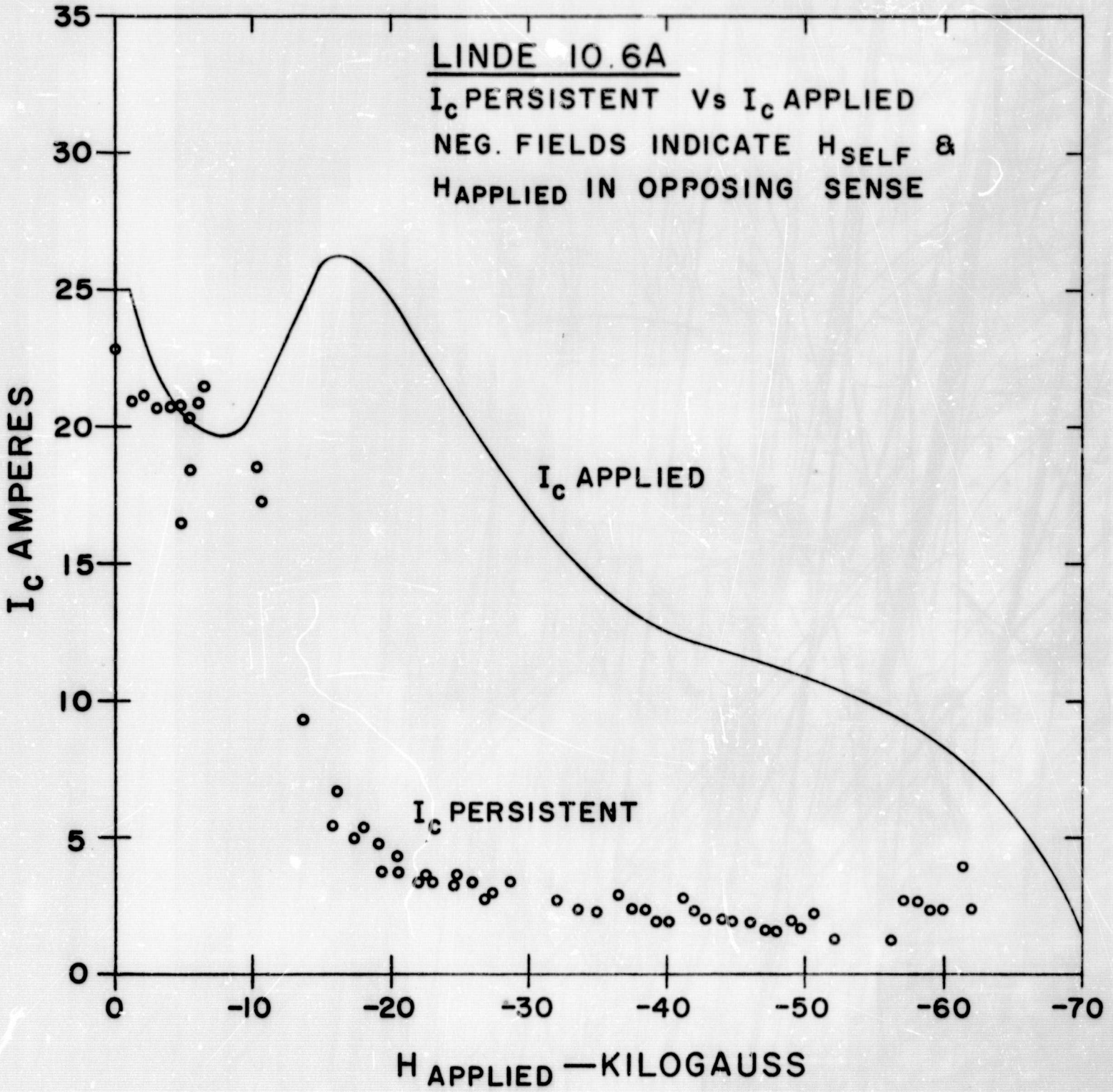

Fig. 3

ORNL DWG. 65-6942

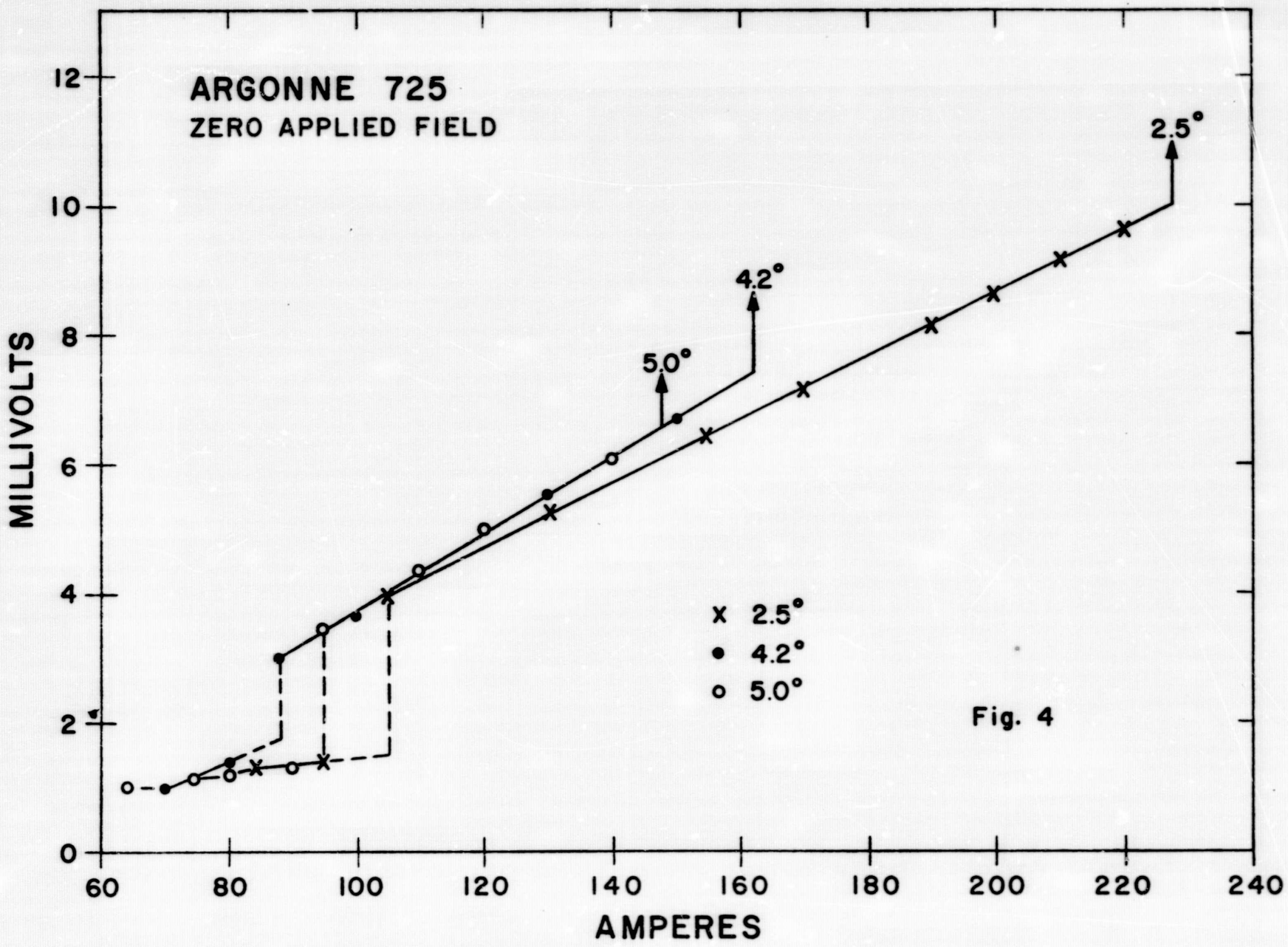

Fig. 4

ORNL DWG. 65-6943

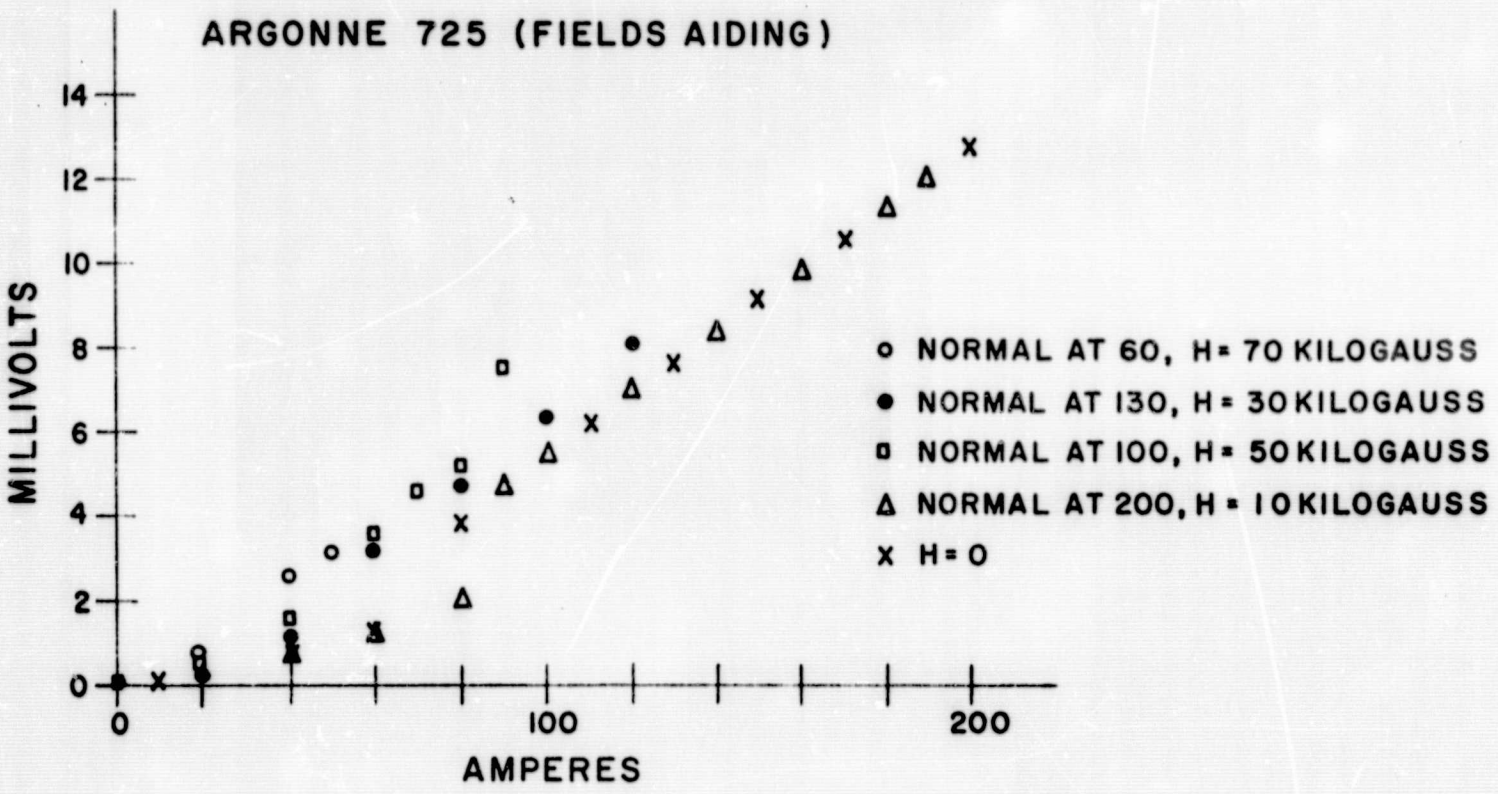

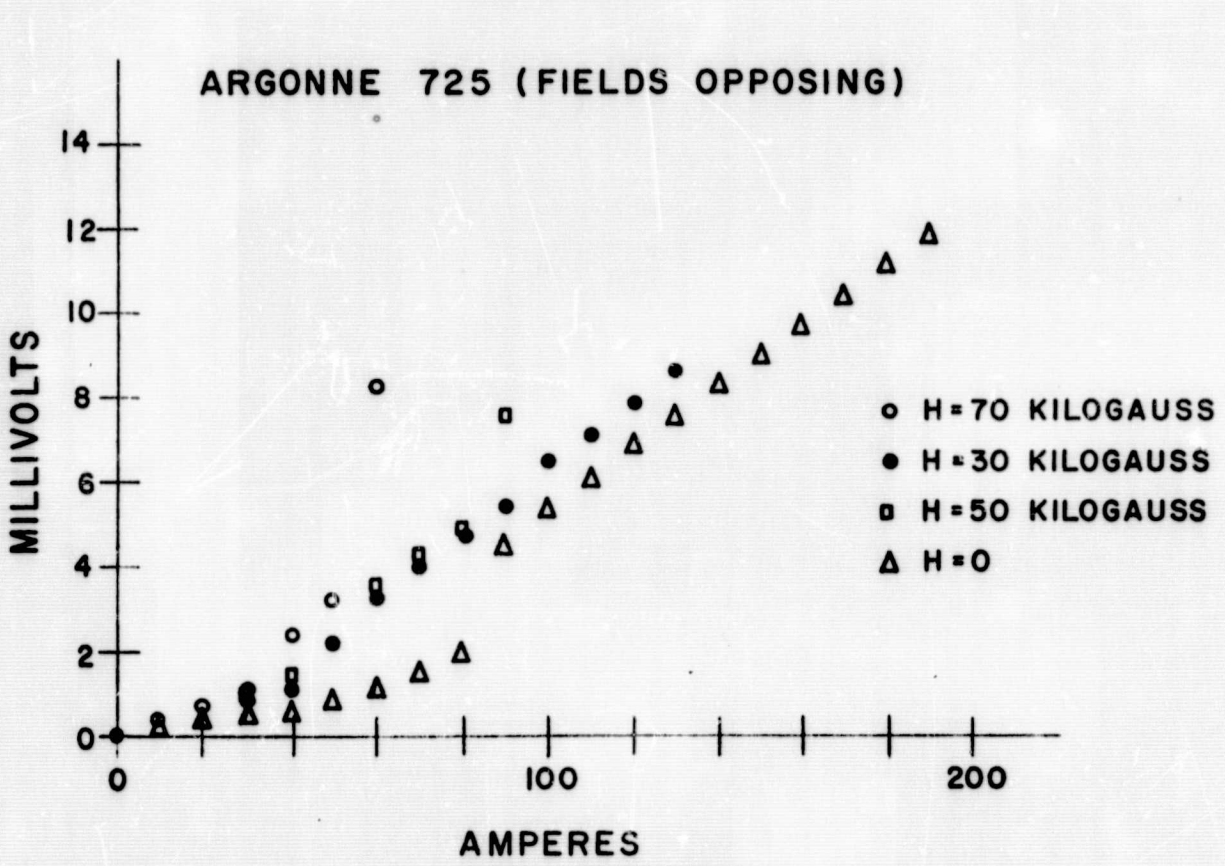

Fig. 5

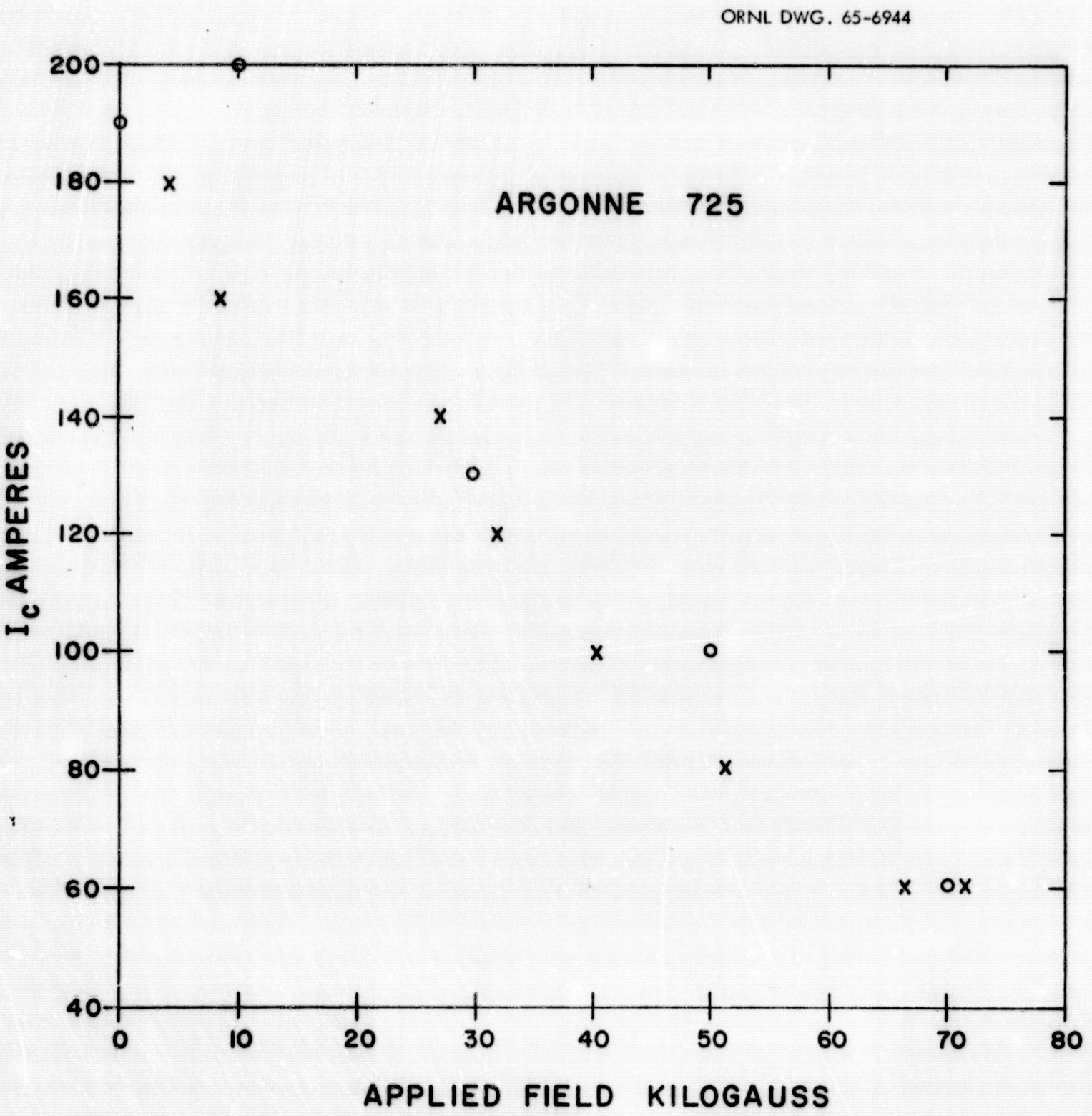
ORNL DWG. 65-6944
ARGONNE 725
I_c AMPERES
200
180
160
140
120
100
80
60
40
0
10
20
30
40
50
60
70
80
APPLIED FIELD KILOGAUSS

Fig. 6

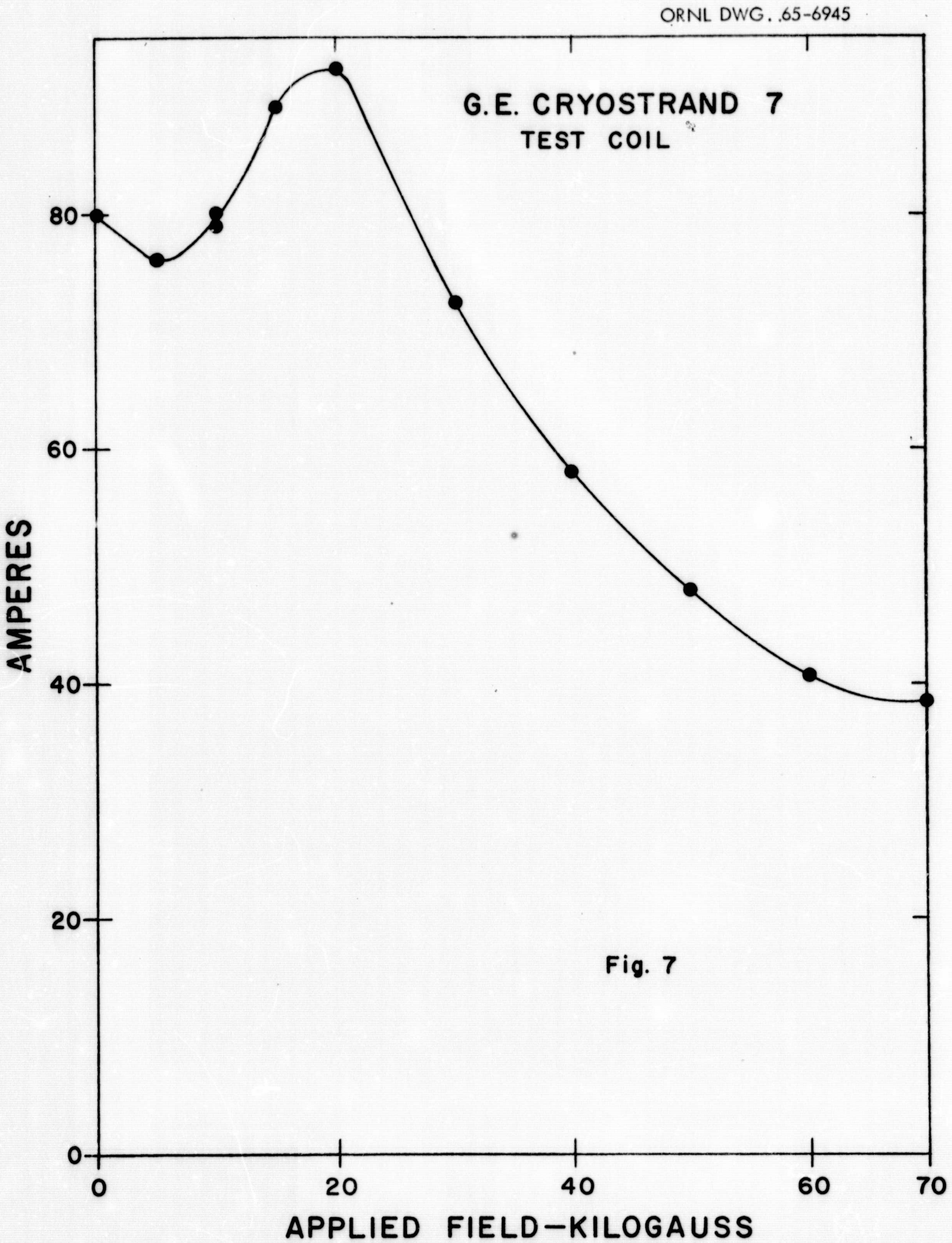
ORNL DWG. 65-6945
G.E. CRYOSTRAND 7
TEST COIL
AMPERES
80
60
40
20
0
0
20
40
60
70
APPLIED FIELD—KILOGAUSS

Fig. 7

Fig. 8

ORNL DWG. 65-6946

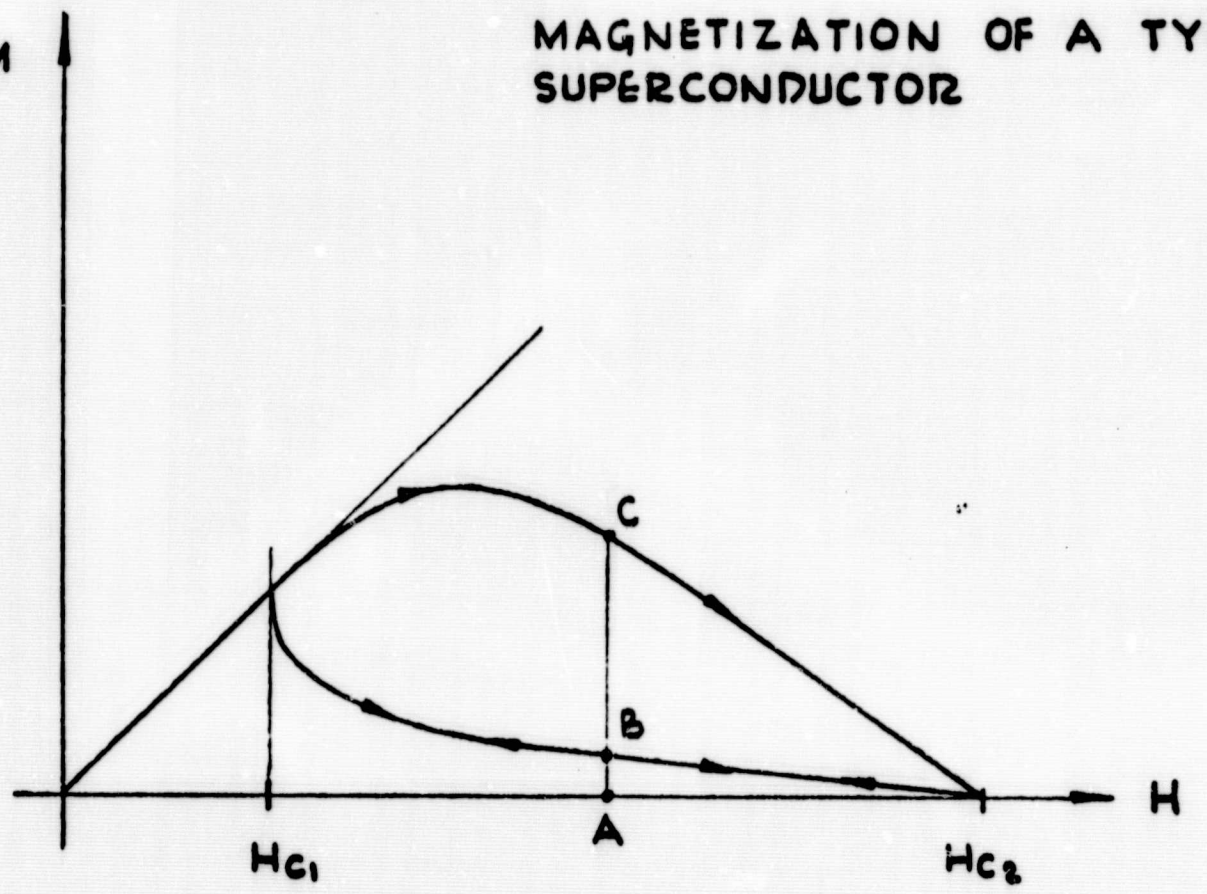

MAGNETIZATION OF A TYPE III SUPERCONDUCTOR

ORNL DWG. 65-6947

Fig. 9

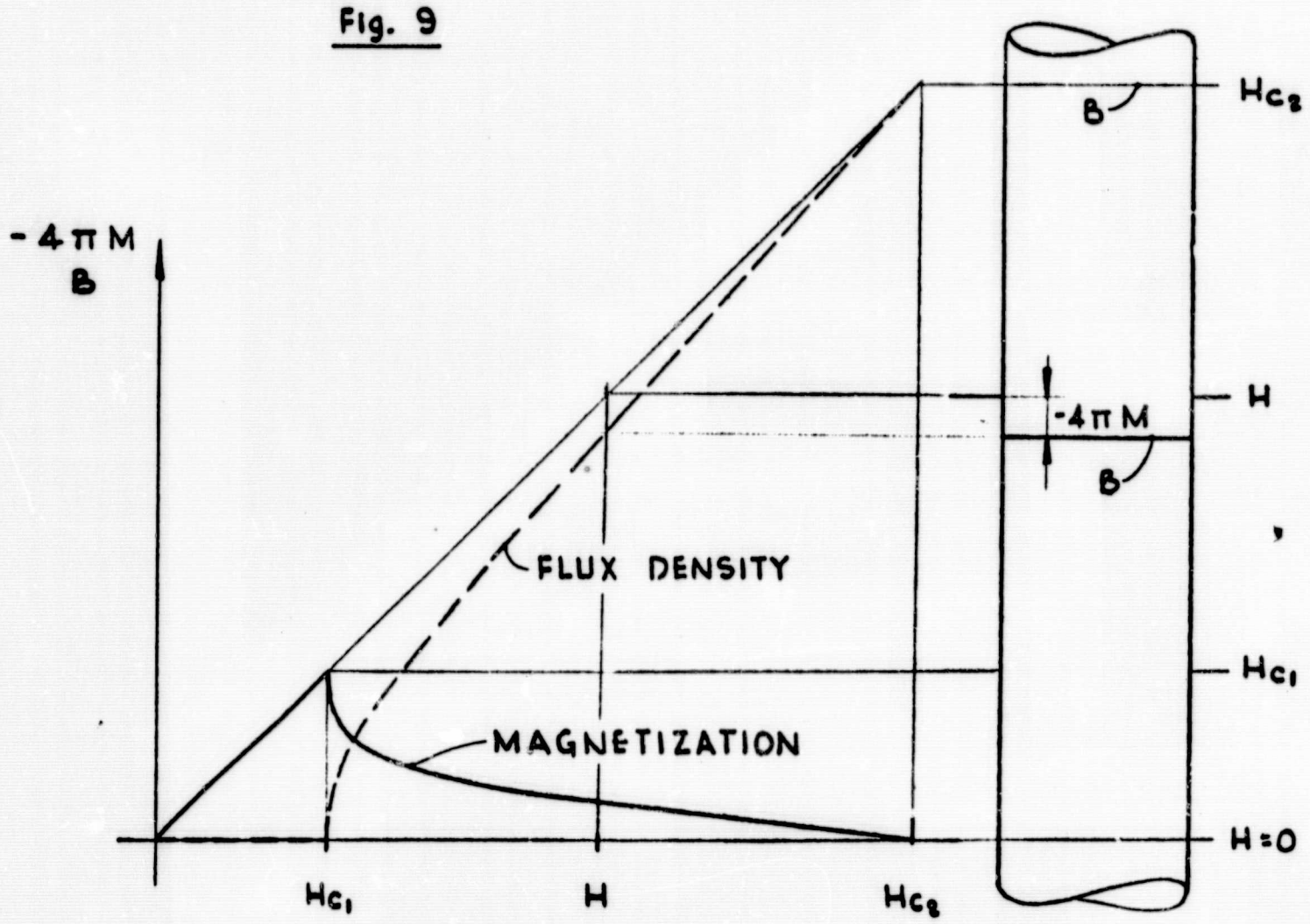

Fig. 9a

Fig. 9b

MAGNETIZATION OF TYPE II SUPERCONDUCTOR

ORNL DWG. 65-6948

Fig. 10

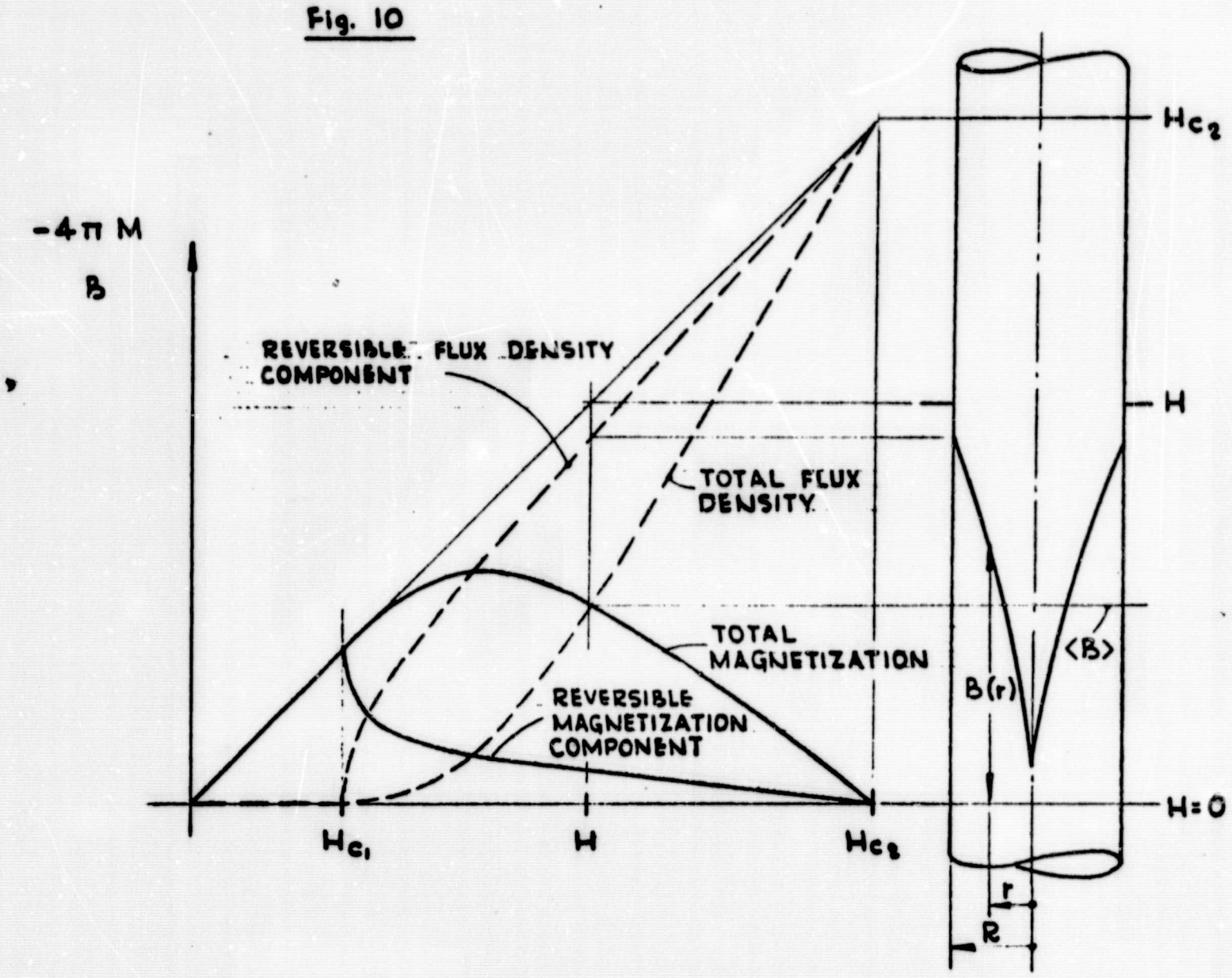

Fig. 10a

Fig. 10b

MAGNETIZATION OF TYPE III SUPERCONDUCTOR

ORNL DWG. 65-6949

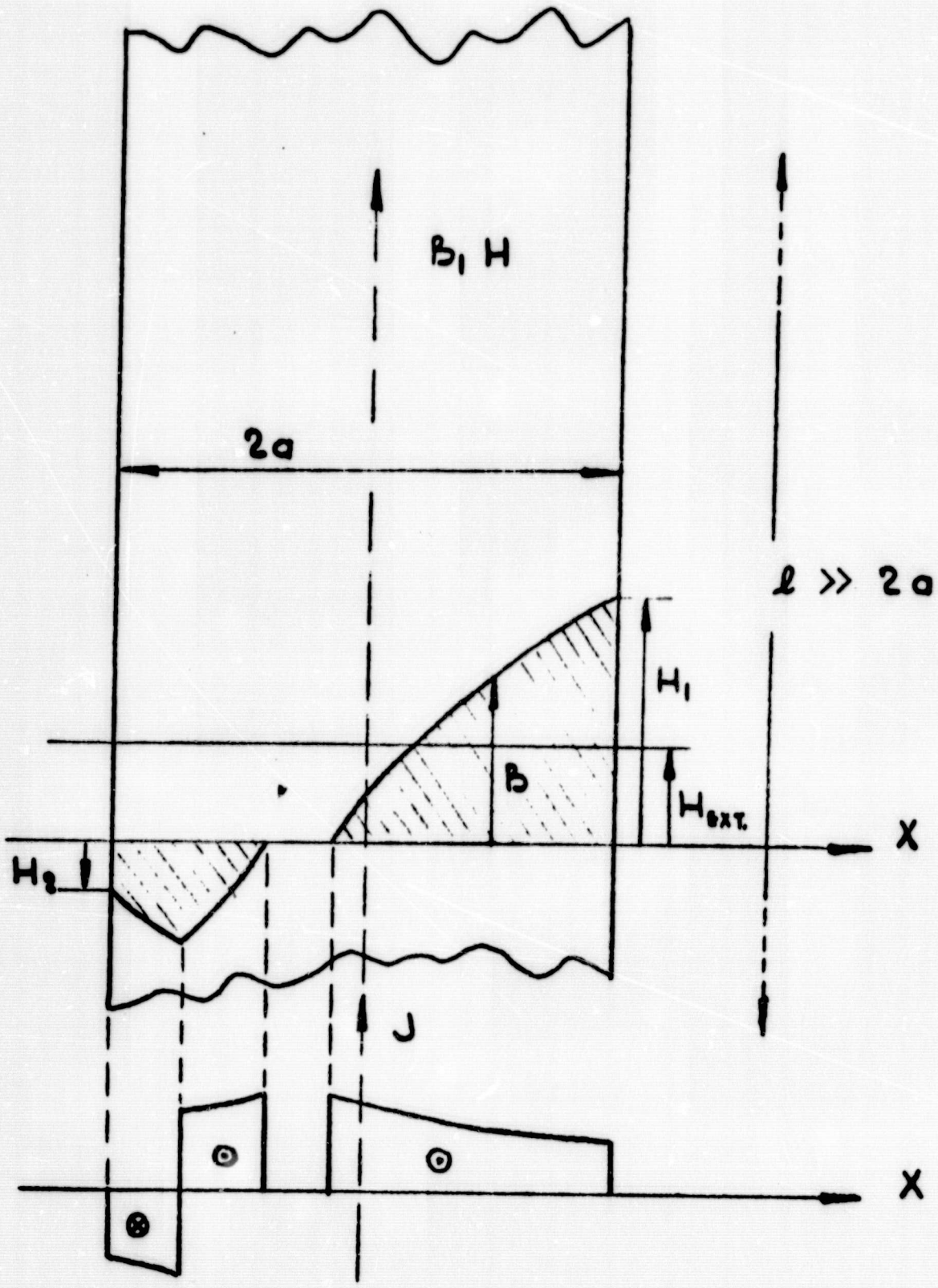

Fig. 11

INFINITE S.C. SLAB IN MAGNETIC FIELD

ORNL DWG. 65-6950

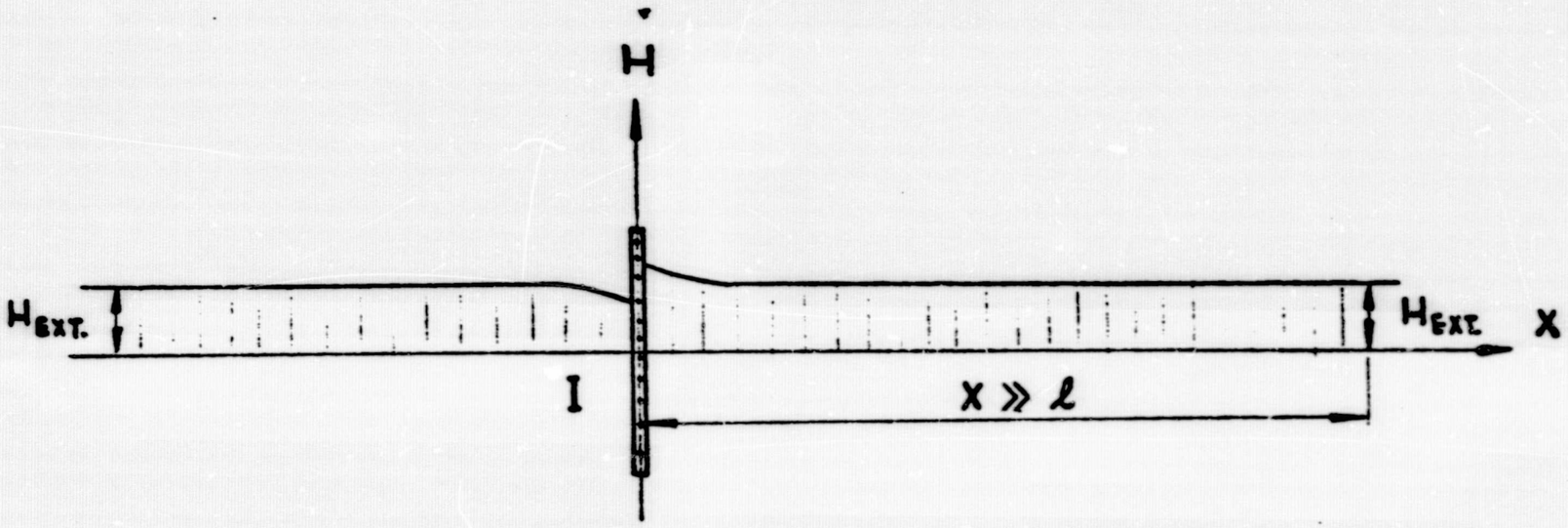

Fig. 12

EFFECT OF CURRENT IN INFINITE S.C. SLAB

ORNL DWG. 65-6951

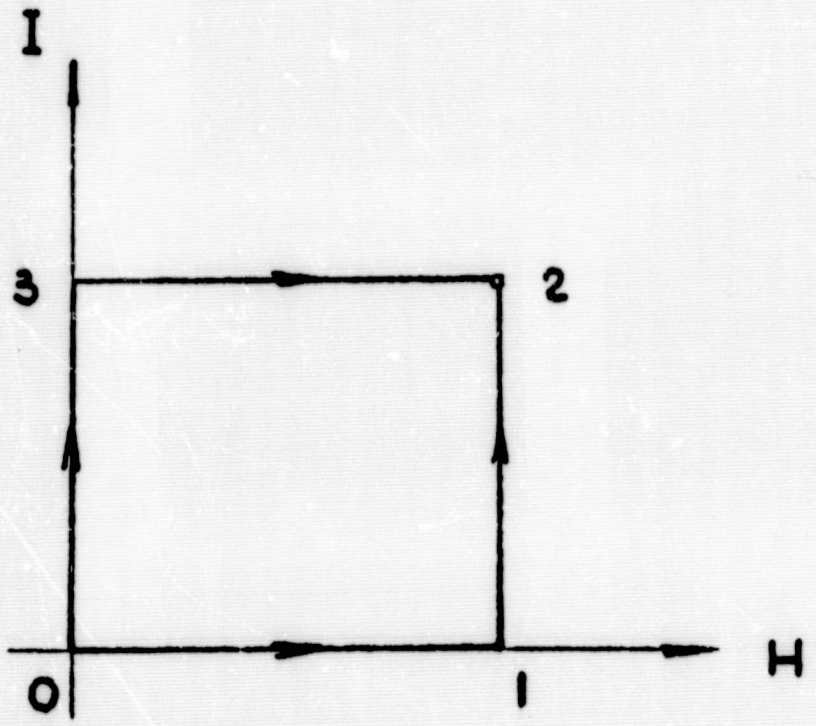

Fig. 13

FIELD AND CURRENT SWEEP MODES

ORNL DWG. 65-6952

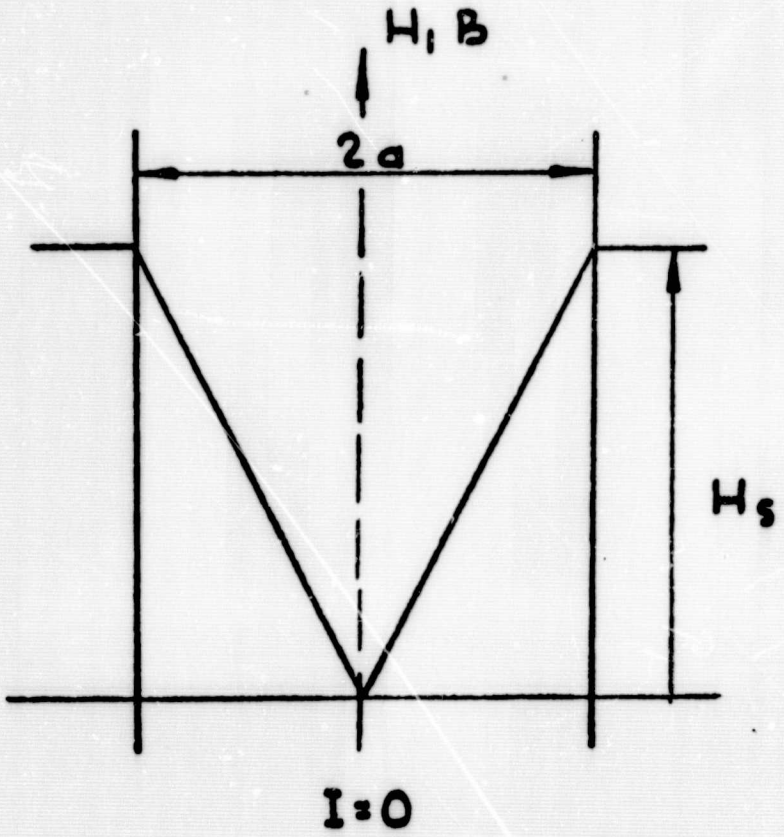

DEFINITION OF H_s

Fig. 14

ORNL DWG. 65-6953

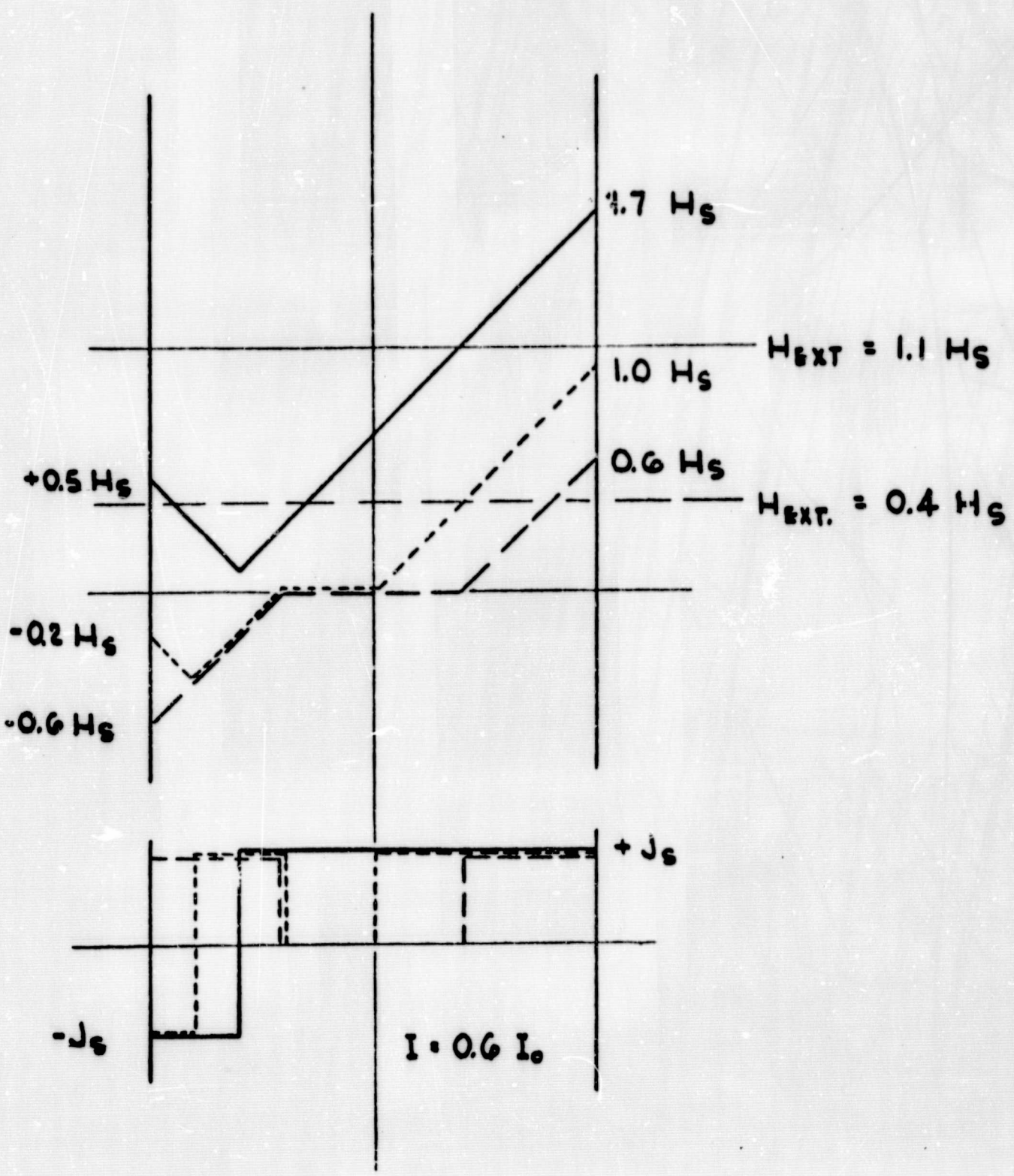

FIELD AND CURRENT DISTRIBUTION FOR SWEEP SEQUENCE I - H

Fig. 15

ORNL DWG. 65-6954

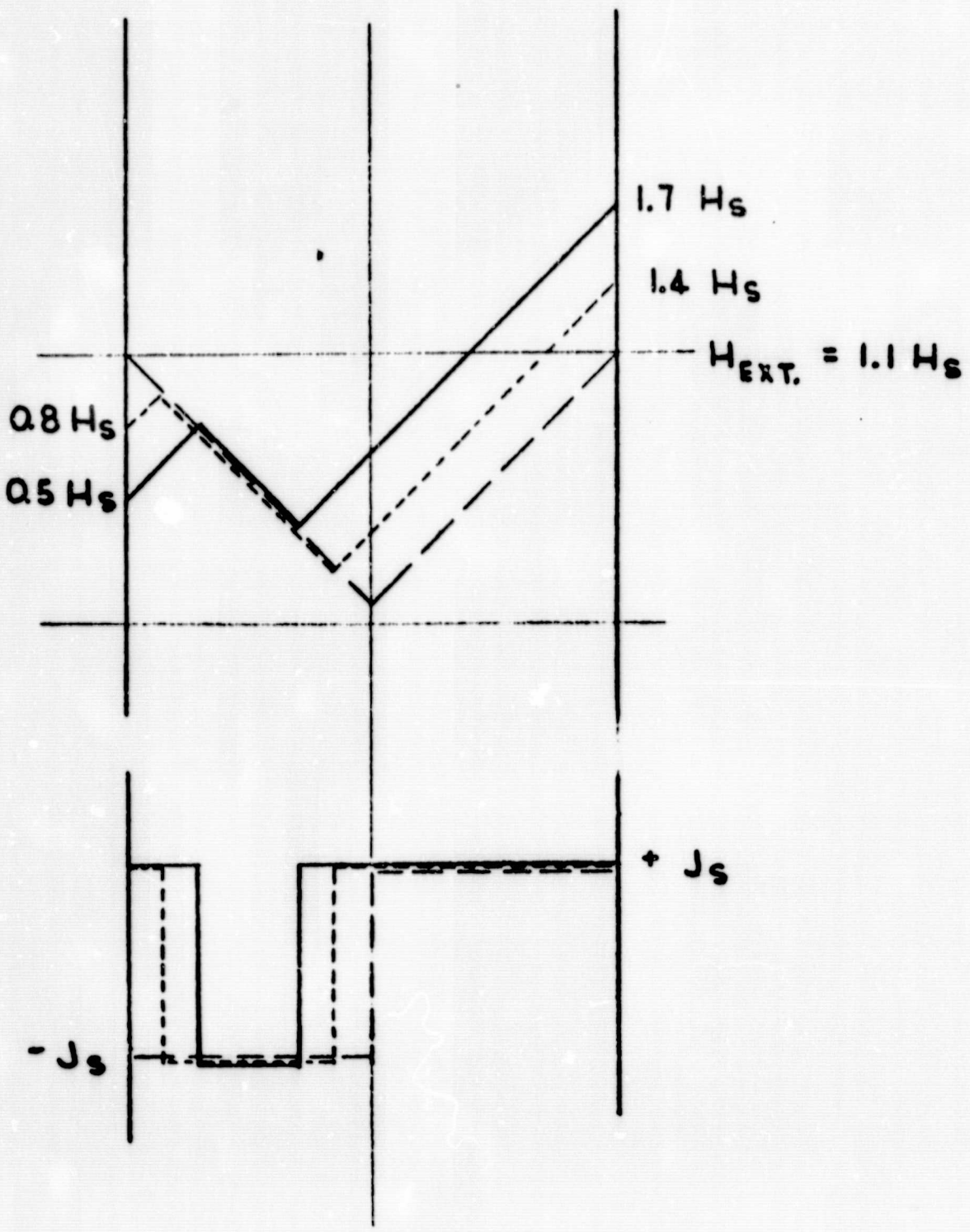

FIELD AND CURRENT DISTRIBUTION FOR SWEEP SEQUENCE H-I

Fig. 16

ORNL DWG. 65-6955

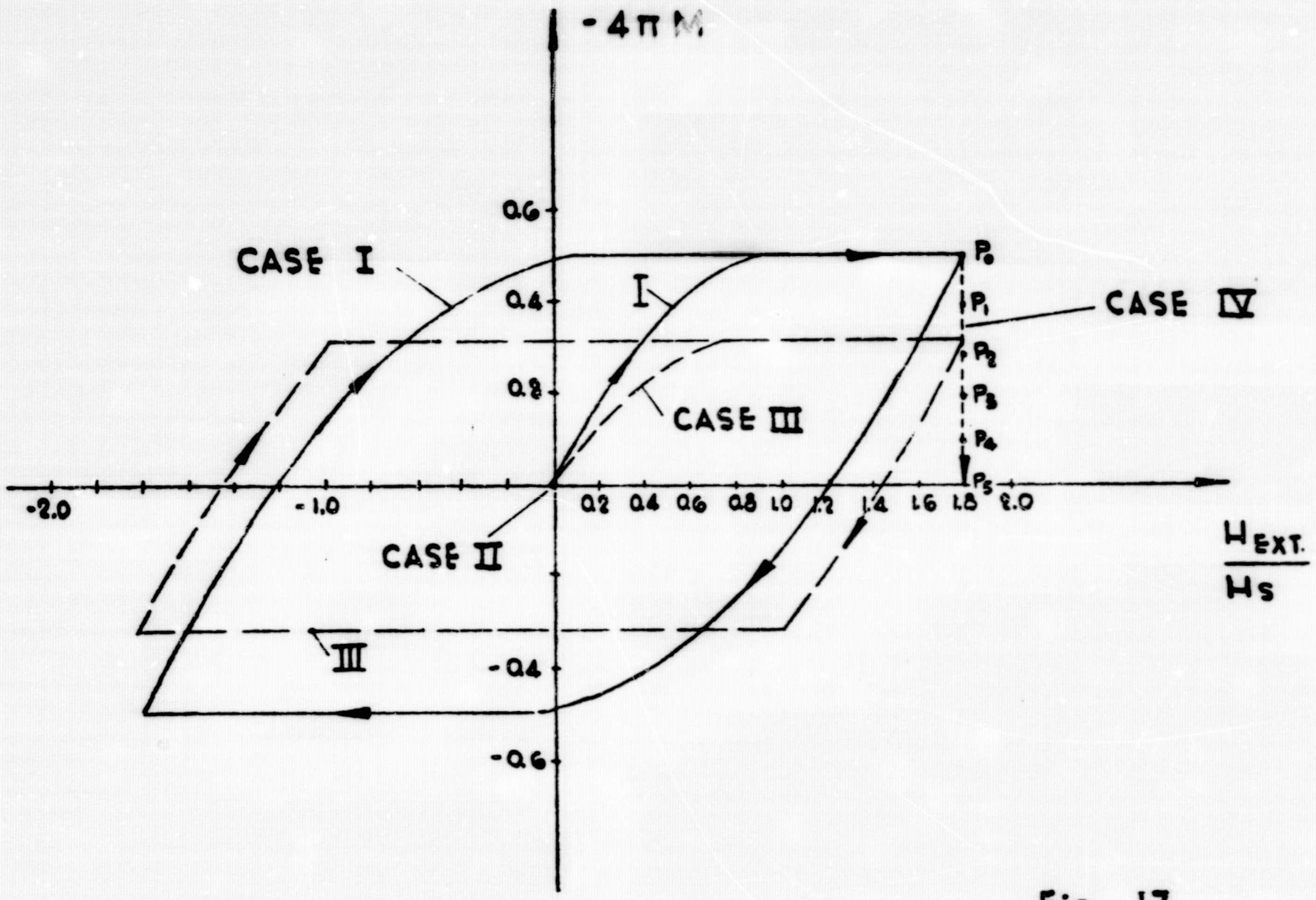

Fig. 17

ORNL DWG. 65-6956

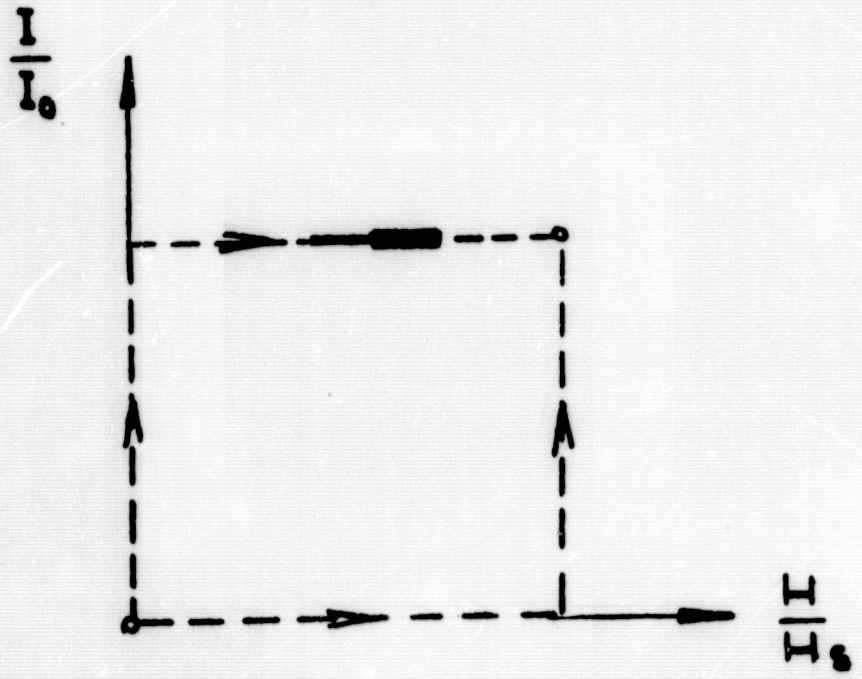

CASE A

Fig. 18

ORNL DWG. 65-6957

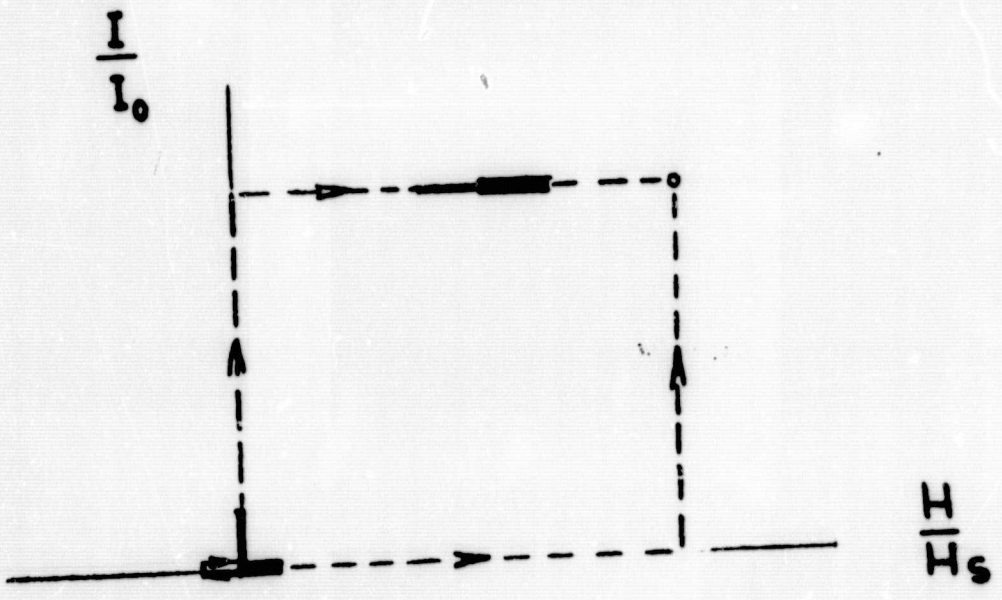

CASE B

Fig. 19

ORNL DWG. 65-6958

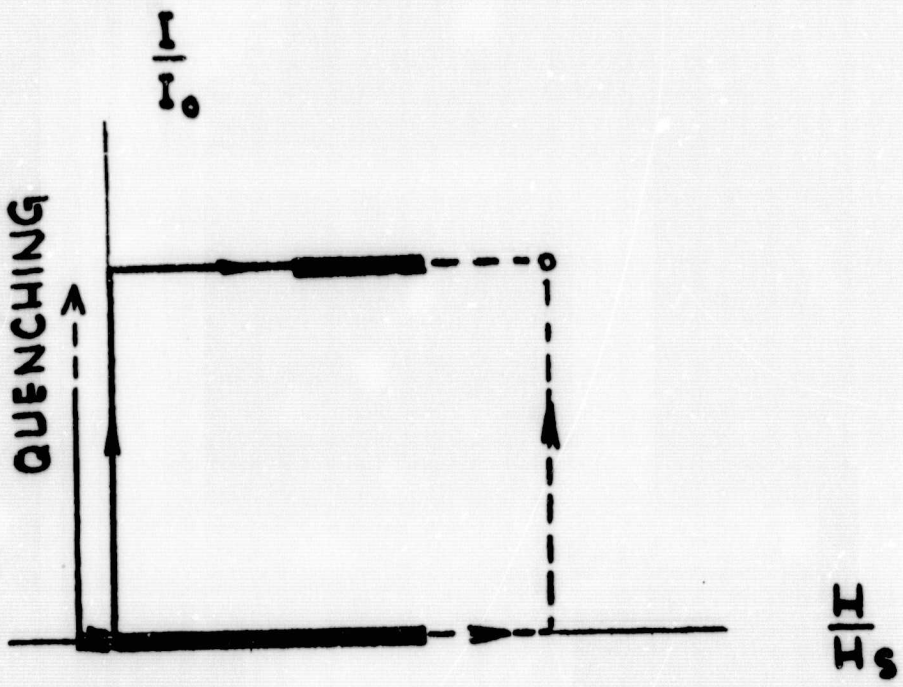

CASE C

Fig. 20

ORNL DWG. 65-6959

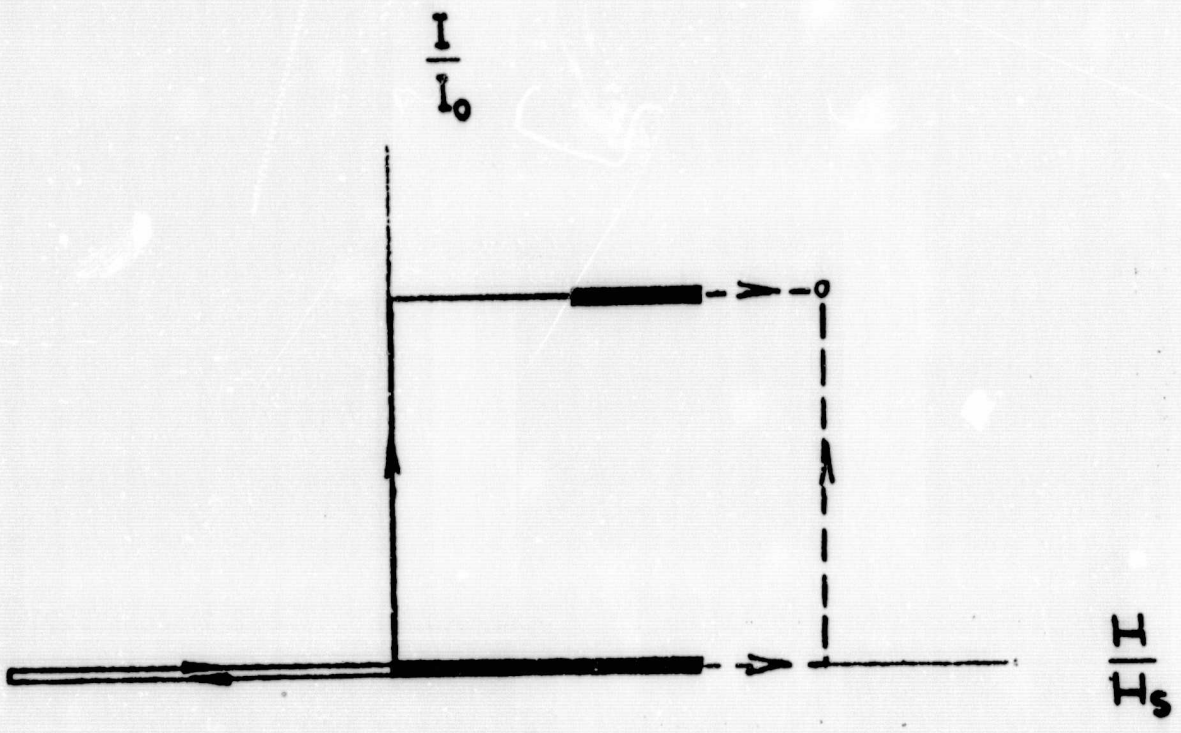

CASE D

Fig. 21

ORNL DWG. 65-6960

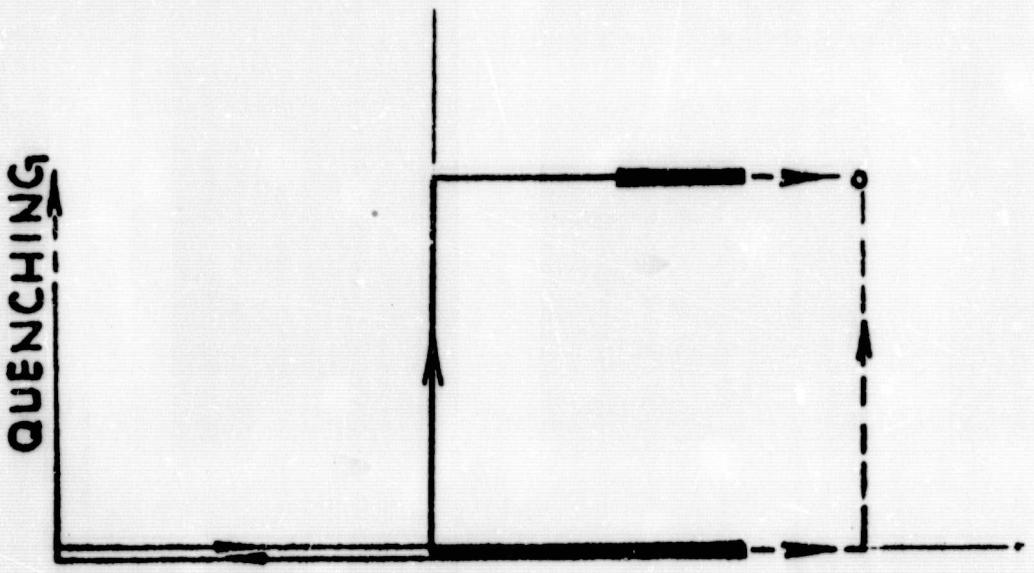

CASE E

Fig. 22

APPENDIX A

A STUDY OF MODELS OF HIGH-FIELD SUPERCONDUCTORS

W. F. Gauster

Reprinted from the Semiannual Progress Report of the Thermonuclear Division of Oak Ridge National Laboratory (period ending October 31, 1963) ORNL - 3564, pp. 107-116. Funded by AEC Activity 05 04 04.

1 Introduction

Simple models of high-field superconductors have been proposed by Heinz London,[1] C. P. Bean,[2] and Y. B. Kim et al.[3,4] They assume that high-field superconductors can carry a critical current density J_c which is either approximately field-independent (London and Bean) or is a function of the local field B (Kim et al.). Bean considers also shielding to a field H_c due to soft superconducting material in the interstices of the mesh. Kim et al. discuss flux trapping ("tube magnetization") and magnetic moment measurements, consider the general properties which follow from their model when any form of the dependence $J_c(B)$ is assumed, and derive from experiments an empirical relation

$$\frac{\alpha}{|J|} = B_o + |B| \tag{1}$$

which is the starting point of P. W. Anderson's theory of the "flux creep" in hard superconductors.[5]

---

[1] Heinz London, private communication: see R. A. Kamper, Phys. Letters 2(6), 290 (1962) and C. P. Bean and R. W. Schmitt, Science 140 (3562), 26 (1963).

[2] C. P. Bean, Phys. Rev. Letters 8(6), 250 (1962).

[3] Y. B. Kim, C. F. Hempstead, and A. R. Strnad, Phys. Rev. Letters 9(7), 306 (1962).

[4] Y. B. Kim, C. F. Hempstead, and A. R. Strnad, Phys. Rev. 129(2), 528 (1963).

[5] P. W. Anderson, Phys. Rev. Letters 9(7), 309 (1962).

This theory has been further developed and extended to resistive states of hard superconductors by Kim et al. in two additional recent publications.[6,7]

The purpose of this study is to give a short systematic presentation of the flux trapping and magnetic moment performance of hollow (and solid) cylinders of hard superconductors in longitudinal fields which are to be expected when the mentioned three different models are used. The forms derived here are partly more comprehensive than those published by other authors to date. Furthermore, this report deals with measurement methods which can be applied for correlating flux trapping and magnetic moment measurements. Experimental results obtained with bundles of copper-plated Nb-Zr wires and a discussion of the applicability of the model of Kim et al. to this special case are presented in the following paper.

2 Heinz London's model of High-Field Superconductors

It is supposed that the critical current density J_c is approximately constant in the entire range of field strength $0 \leq H \leq H_M$. No perfect flux exclusion at low fields is assumed. The simplest case of a hollow or solid cylinder cooled in zero field is considered here.

Figure 1 shows the current distribution inside the tube wall for six phases of a magnetization cycle if a homogeneous external field H parallel to the cylinder axis is applied. The corresponding internal field distribution is represented by Fig. 2. When H is raised to a moderate value H_I, the field B inside the tube wall decreases linearly (curve I), becomes zero at a distance R_I from the outside surface of the tube, and for $R_I \leq R \leq w$ the field $B = 0$ (curve I'). For $H = H_{II}$, the field penetrates over the entire wall thickness w. If the external field is raised to a maximum H_M and then lowered to H_{III}, currents in the opposite direction are supposed

---

[6] Y. B. Kim, C. F. Hempstead, and A. R. Strnad, "Resistive States of Hard Superconductors," Rev. Mod. Phys. 36 (1), 43 (1964).

[7] Y. B. Kim, C. F. Hempstead, and A. R. Strnad, Phys. Rev. 131(6), 2486 (1963).

to propogate inward from the outer surface to a distance R_{III}. The currents for $R > R_{III}$ remain unchanged and the field distribution III-III' (Fig. 2) results. When H is lowered to H_{IV}, the whole tube wall carries currents in the opposite direction. For $H = H_V$ the external field becomes negative; the field H'_V inside the tube is still positive. For a still lower value $H = H_{VI}$, the state represented by curve II is inverted.

The flux trapping or tube magnetization curve[3] (i.e., the H – H' diagram) is shown in Fig. 3. It must be emphasized, however, that it is very difficult to achieve complete magnetization cycle measurements with high-field superconducting cylinders or tubes, since "flux jumps" might occur.[4]

The field distribution inside the tube for the cases I to VI can be easily calculated. We first consider case II (Figs. 1 and 2):

$$B = H - \frac{4\pi}{10} J_c R \,. \tag{2}$$

The distance R is measured from the outside surface of the hollow cylinder. Introducing the designations

$$\frac{4\pi}{10} = k, \quad kJ_c w = H^*, \quad \frac{H}{H^*} = h, \quad \frac{B}{H^*} = b, \quad \frac{R}{W} = r, \tag{3}$$

we obtain

$$b = h - r, \tag{4}$$

and

$$b(r = 0) = h; \quad b(r = 1) = h' = h - 1. \tag{5}$$

The corresponding equations for cases I to VI are listed in Table 1. Obviously the normalization of the quantities used simplifies the notation very much.

The current and field distribution inside the tube wall is independent of the magnitude of the inside radius a − w of the hollow cylinder. This does not hold, however, for the average magnetic moment per unit volume $\bar{M}$ of the superconducting tube:

$$-4\pi\bar{M} = \frac{1}{\pi(a^2 - (a - w)^2)} \int_{R=0}^{w} 2\pi(a - R)(H - B)\, dR. \quad (6)$$

In normalized form (with a = Kw)

$$-4\pi\bar{m} = -4\pi \frac{\bar{M}}{H^*} = \frac{2}{2K - 1} \int_{r=0}^{1} (K - r)(h - b)\, dr\ . \quad (7)$$

For a thin-walled tube $K \to \infty$; for a solid cylinder K = 1. Another convenient form of Eq. (7) is

$$-4\pi\bar{m} = h - \bar{b}\ , \quad (7a)$$

$$\bar{b} = \frac{2}{2K - 1} \int_{r=0}^{1} (K - r)b\, dr\ .$$

Normalized magnetic moment values, based on Heinz London's model, are listed in Table 2; moment curves are shown in Fig. 4. Here h_m is assumed to be equal to 4.0. The maximum normalized magnetic moment magnitude is 1/2 for a thin-walled tube (or a slab of hard superconducting material), and 1/3 for a solid cylinder. Even for very small values of the external field H, the magnetic moment is not reversible. For large external field values the magnetic moment does not decrease.

3 C. P. Bean's Model[8]

Normalized values are again used (Eq. (3)). The normalized critical field strength in the interstices of the filaments is

$$h_c = \frac{H_c}{H^*} . \tag{8}$$

Field distributions for four characteristic cases are listed in Table 3. Cases (c), (d), and (e) are identical with cases II, III, and IV, respectively, of London's model. No values are shown for h decreasing and $h < h_c$ since in this case an interpretation of Bean's model is not obvious. In Fig. 5 magnetic moment curves of solid cylinders and thin-walled tubes are compared for H* equal to H_c, $3H_c$, and $10H_c$, respectively. The curves for solid cylinders are identical with those shown in Bean's paper[8] (solid lines). The curves for the thin-walled tubes represent cases (a), (b), and (c) for $K \to \infty$ of Table 4 (dashed lines).

4 Model of Y. B. Kim et al.

If the model of Kim et al.[9,10] is used, Eq. (1) combined with

$$dB = kJ\, dR, \tag{9}$$

determines the critical current and field distributions in high-field superconductor tubes which are exposed to homogeneous longitudinal external fields. We use normalized designations similar to Eq. (3); however, field values are now divided by

$$H_w = \sqrt{2\alpha k w} \tag{10}$$

---

[8] C. P. Bean, Phys. Rev. Letters 8(6), 250 (1962).

[9] Y. B. Kim, C. F. Hempstead, and A. R. Strnad, Phys. Rev. Letters 9(7), 306 (1962).

[10] Y. B. Kim, C. F. Hempstead, and A. R. Strnad, Phys. Rev. 129 (2), 528 (1963).

rather than by H^*. Corresponding to the cases I to IV, shown for London's model in Figs. 1 and 2, field distributions for the model of Kim et al. can be easily calculated. They are listed in Table 5. The resulting tube magnetization curves for a complete magnetization cycle (no flux jumps considered!) are shown in Fig. 6 (compare ref. 9).

Using Eqs. (7) or (7a), the magnetic moment values for cases I to VI can be easily computed. A straightforward integration of Eq. (7a) with respect to b, using the r(b) values (easily calculated from Table 5) yields the $\bar{b}$ values listed in Table 6. The equation for case I is very simple, since the higher limit of the integration is h = 0. For the other cases, the forms listed in Table 6 can be simplified if, instead of b, the variable

$$u = h - b \tag{11}$$

is introduced, which becomes equal to zero at the lower limit of intergration. For instance, in case II, r can be written in the form

$$\begin{aligned} r &= (b_o + h)^2 - (b_o + b)^2 = u(v - u), \\ v &= 2(b_o + h). \end{aligned} \tag{12}$$

These values introduced in Eq. (7) yield

$$-4\pi\bar{m} = \frac{u_1^2}{2K - 1}\left[Kv - \frac{2}{3}(2K + v^2)\, u_1 + \frac{3v}{2}u_1^2 - \frac{4}{5}u_1^3\right], \tag{13}$$

$$u_1 = u(b = h') = h - h'$$

Equations in normalized form are convenient if the quantities B_0 and α have been determined by tube magnetization measurements and magnetic moment curves are to be calculated. For the direct evaluations of magnetic moment measurements nonnormalized equations are preferable. It is easy to rewrite Eq. (13), for instance, in a nonnormalized form. Introducing

$$U_1 = H_w u_1 = H - B$$
$$V = H_w v = 2(B_o + H) \ , \tag{14}$$

we obtain from Eq. (13)

$$-4\pi\overline{M} = \frac{1}{(2K-1)\ H_w^2}\left[\ KVH_w^2 - \frac{2}{3}\ (2KH_w^2 + V^2)U_1 + \frac{3}{2}\ VU_1^2 - \frac{4}{5}\ U_1^3\ \right] . \tag{15}$$

Equation (12) can be written as

$$H_w^2 = U_1\ (V - U_1),$$

and therefore

$$-4\pi\overline{M} = \frac{1}{(2K-1)(V-U_1)}\left[\left(K - \frac{2}{3}\right)V^2\right.$$
$$\left.-\left(\frac{7}{3}K - \frac{3}{2}\right)U_1V + \left(\frac{4}{3}K - \frac{4}{5}\right)U_1^2\ \right] .$$

Using the abbreviation

$$\nu = \frac{H' - H}{B_o + H}$$

we obtain

$$-4\pi\bar{M} = \frac{2}{3}\,\frac{H - H'}{(2K-1)(2+\nu)^2}\left[2\left(K - \frac{3}{5}\right)\nu^2 + \left(7K - \frac{9}{2}\right)\nu + 2(3K-2)\right]. \tag{19}$$

and an expression for the magnetic moment in case II for arbitrary values of K. For K = 1, Eq. (14) of the paper of Kim et al.[10] follows:

$$-4\pi\bar{M} = \frac{H - H'}{15(2+\nu)^2}\,(8\nu^2 + 25\nu + 20). \tag{20}$$

For a thin-walled tube (or a slab of high-field superconducting material), $K \to \infty$, and Eq. (19) becomes

$$-4\pi\bar{M} = \frac{1}{3}\,\frac{H - H'}{(2+\nu)^2}\,(2\nu^2 + 7\nu + 6). \tag{21}$$

Magnetic moment curves for a complete magnetization cycle (cases I to VI), calculated for $b_o = 0.7$ and $K = \infty$, 2, and 1, respectively, are shown in Fig. 7. Nonnormalized forms for $\bar{M}$, for cases I to V, valid for any ratios of outside to inside tube radii are listed in Table 7 of the following paper, which reports on magnetic moment measurements of bundles of copper-plated Nb-Zr wires and discusses the application of the model of Kim et al. to the results.

4 Acknowledgments

The author wishes to acknowledge the most useful discussions with D. C. Hopkins and the invaluable assistance of C. E. Parker, who made the numerical calculations for Fig. 8.

Table 1. Heinz London's Model: Field Distribution

I	h increasing	$0 \leq h \leq h_s$; $h_s = 1$; $r_I = h$; $h' = 0$	
	$0 \leq r \leq r_I$	$b = h - r$	
	$r_I \leq r \leq 1$	$b = 0$	
II	h increasing	$h_s \leq h \leq h_M$; $h' = h - 1$; $h'_M = h_m - 1$; $b = h - r$	
III	h decreasing	$h_m \leq h \leq h_M$; $h_m = h_M - 2$; $h' = h'_M$	
		$r_{III} = \frac{1}{2}(h_M - h)$; $b_{III} = \frac{1}{2}(h_M + h)$	
	$0 \leq r \leq r_{III}$	$b = h + r$	
	$r_{III} \leq r \leq 1$	$b = h_M - r$	
IV	h decreasing	$0 \leq h \leq h_m$	$h' = h + 1$; $b = h + r$
V	h decreasing	$-h_s \leq h \leq 0$	
VI	h decreasing	$-h_M \leq h \leq -h_s$	

Table 2. Heinz London's Model: Values for $-4\pi\bar{m}$

Case	Hollow Cylinder	Thin-Wall Tube	Solid Cylinder
I	$h - \frac{K}{2K - 1} h^2 + \frac{1}{6K - 3} h^3$	$h - \frac{h^2}{2}$	$h - h^2 + \frac{h^3}{3}$
II	$\frac{3K - 2}{6K - 3}$	$\frac{1}{2}$	$\frac{1}{3}$
III	$\frac{3K - 2}{6K - 3} - (h_M - h) + \frac{1}{6K - 3} \times \left[\frac{3K}{2} (h_M - h)^2 - \frac{1}{4} (h_M - h)^3 \right]$	$\frac{1}{2} - (h_M - h) + \frac{(h_M - h)^2}{4}$	$\frac{1}{3} - (h_M - h) + \frac{(h_M - h)^2}{2} - \frac{(h_M - h)^3}{12}$
IV, V, VI	$- \frac{3K - 2}{6K - 3}$	$- \frac{1}{2}$	$- \frac{1}{3}$

Table 3. C. P. Bean's Model: Field Distribution

Case (a)	h increasing	$0 \leq h < h_c$; $b = h' = 0$
Case (b)	h increasing	$h_c < h < h_c + 1$; $r_b = h - h_c$
	$0 < r < r_b$	$b = h - r$
	$r_b < r < 1$	$b = 0$
Case (c)	h increasing	$h_c + 1 < h \leq h_M$; $h_M > h_c + 2$
		$b = h - r$; $h' = h - 1$; $h'_M = h_M - 1$
Case (d)	h decreasing	$h_m \leq h \leq h_M$; $h_m = h_M - 2$; $h' = h'_M$
		$r_d = \frac{1}{2}(h_M - h)$; $b_d = \frac{1}{2}(h_M + h)$
	$0 \leq r \leq r_d$	$b = h + r$
	$r_d \leq r \leq 1$	$b = h_M - r$
Case (e)	h decreasing	$h_c \leq h \leq h_m$; $b = h + r$; $h' = h + 1$

Table 4. C. P. Bean's Model: Values for $-4\pi\bar{m}$

Case	Hollow Cylinder	Thin-Wall Tube	Solid Cylinder
(a)	h	h	h
(b)	$h - \frac{2}{2K-1}\left[Kh(h-h_c) - (K+h) \times \frac{(h-h_c)^2}{2} + \frac{(h-h_c)^3}{3}\right]$	$h - \frac{h^2 - h_c^2}{2}$	$h - (h-h_c)\left[h_c + h - h(h-h_c) + \frac{2}{3}(h-h_c)^2\right]$
(c)		Table 2, Case II	
(d)		Table 2, Case III	
(e)		Table 2, Case IV	

Table 5. Model of Y. B. Kim et al.: Field Distribution

I h increasing: $0 \le h \le h_s$; $h_s = \sqrt{b_o^2 + 1} - b_o$; $r_I = 2\, b_o\, h + h^2$; $h' = 0$

$0 \le r \le r_I$ $b = \sqrt{(b_o + h)^2 - r} - b_o$; $r = (b_o + h)^2 - (b_o + b)^2$

$r_I \le r \le 1$ $b = 0$

II h increasing: $h_s \le h \le h_M$; $h' = \sqrt{(b_o + h)^2 - 1} - b_o$; $h'_M = \sqrt{(b_o + h_M)^2 - 1} - b_o$

$b = \sqrt{(b_o + h)^2 - r} - b_o$; $r = (b_o + h)^2$

III h decreasing: $h_m \le h \le h_M$; $h_m = \sqrt{(b_o + h_M)^2 - 2} - b_o$; $h' = h'_M$

$r_{III} = \frac{1}{2}\left[(b_o + h_M)^2 - (b_o + h)^2\right]$; $b_{III} = \sqrt{\frac{1}{2}\left[(b_o + h_M)^2 + (b_o + h)^2\right]} - b_o$

$0 \le r \le r_{III}$ $b = \sqrt{(b_o + h)^2 + r} - b_o$; $r = (b_o + b)^2 - (b_o + h)^2$

$r_{III} \le r \le 1$ $b = \sqrt{(b_o + h_M)^2 - r} - b_o$; $r = (b_o + h_M)^2 - (b_o + b)^2$

IV h decreasing: $0 \le h \le h_M$; $h' = \sqrt{(b_o + h)^2 + 1} - b_o$

$b = \sqrt{(b_o + h)^2 + r} - b_o$; $r = (b_o + b)^2 - (b_o + h)^2$

V h decreasing: $-h_s \le h \le 0$; $h' = \sqrt{1 + 2\, b_o^2 - (b_o - h)^2} - b_o$

$r_v = (b_o - h)^2 - b_o^2$; $b_v = 0$

$0 \le r \le r_v$ $b = b_o - \sqrt{(b_o - h)^2 - r}$; $r = (b_o - h)^2 - (b_o - b)^2$

$r_v \le r \le 1$ $b = \sqrt{(b_o + h')^2 + r - 1} - b_o$; $r - (b_o + b)^2 - (b_o - h)^2 - 2\, b_o^2$

VI h decreasing: $h_s \le -h_s$; $h' = b_o - \sqrt{(b_o - h)^2 - 1}$

$b = b_o - \sqrt{(b_o - h)^2 - r}$

Table 6. Model of Y. B. Kim et al.: Values of $(2K - 1)\bar{b}$
$(-4\pi\bar{m} = h - \bar{b})$

I	$h^2[2b_oK + \frac{4}{3}(K - b_o)^2h - \frac{5}{3}b_oh^2 - \frac{8}{15}h^3]$
II	$[2b_o(K - 2b_oh - h^2)b^2 + \frac{4}{3}(K + 2b_o^2 - 2b_oh - h^2)b^3 + 3b_ob^4 + \frac{4}{5}b^5]_{b=h'}^{h}$
III	$[2b_o(K + 2b_oh + h^2)b^2 + \frac{4}{3}(K - 2b_o^2 + 2b_oh + h^2)b^3 - 3b_ob^4 - \frac{4}{5}b^5]_{b=h}^{b_m} +$ $[2b_o(K - 2b_oh_M - h_M^2)b^2 + \frac{4}{3}(K + 2b_o^2 - 2b_oh_M - h_M^2)b^3 + 3b_ob^4 + \frac{4}{5}b^5]_{b=h_M'}^{b_m}$
IV	$[2b_o(K + 2b_oh + h^2)b^2 + \frac{4}{3}(K - 2b_o^2 + 2b_oh + h^2)b^3 - 3b_ob^4 - \frac{4}{5}b^5]_{b=h}^{h'}$
V	$[2b_o(K + 2b_oh - h^2)b^2 - \frac{4}{3}(K + 2b_o^2 + 2b_oh - h^2)b^3 + 3b_ob^4 - \frac{4}{5}b^5]_{b=h}^{0} +$ $[2b_o(K + 2b_oh' + h'^2 - 1)b^2 + \frac{4}{3}(K - 2b_o^2 + 2b_oh' + h'^2 - 1)b^3 -$ $3b_ob^4 - \frac{4}{5}b^5]_{b=0}^{h'}$
VI	$[2b_o(K + 2b_oh - h^2)b^2 - \frac{4}{3}(K + 2b_o^2 + 2b_oh - h^2)b^3 + 3b_ob^4 - \frac{4}{5}b^5]_{b=h}^{h'}$

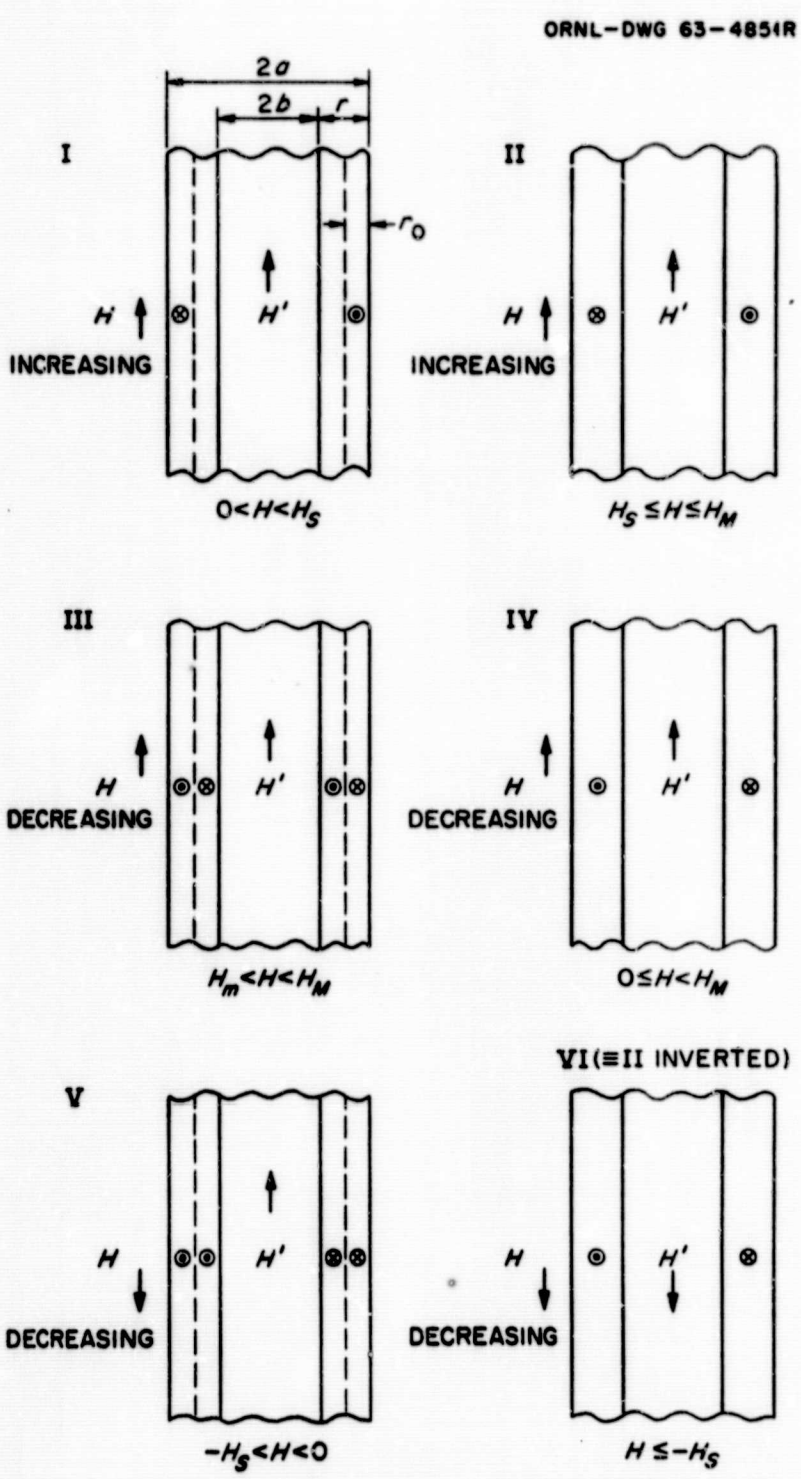

Fig. 1. Current Distribution in a High-Field Superconductor Tube for Different States of a Magnetization Cycle.

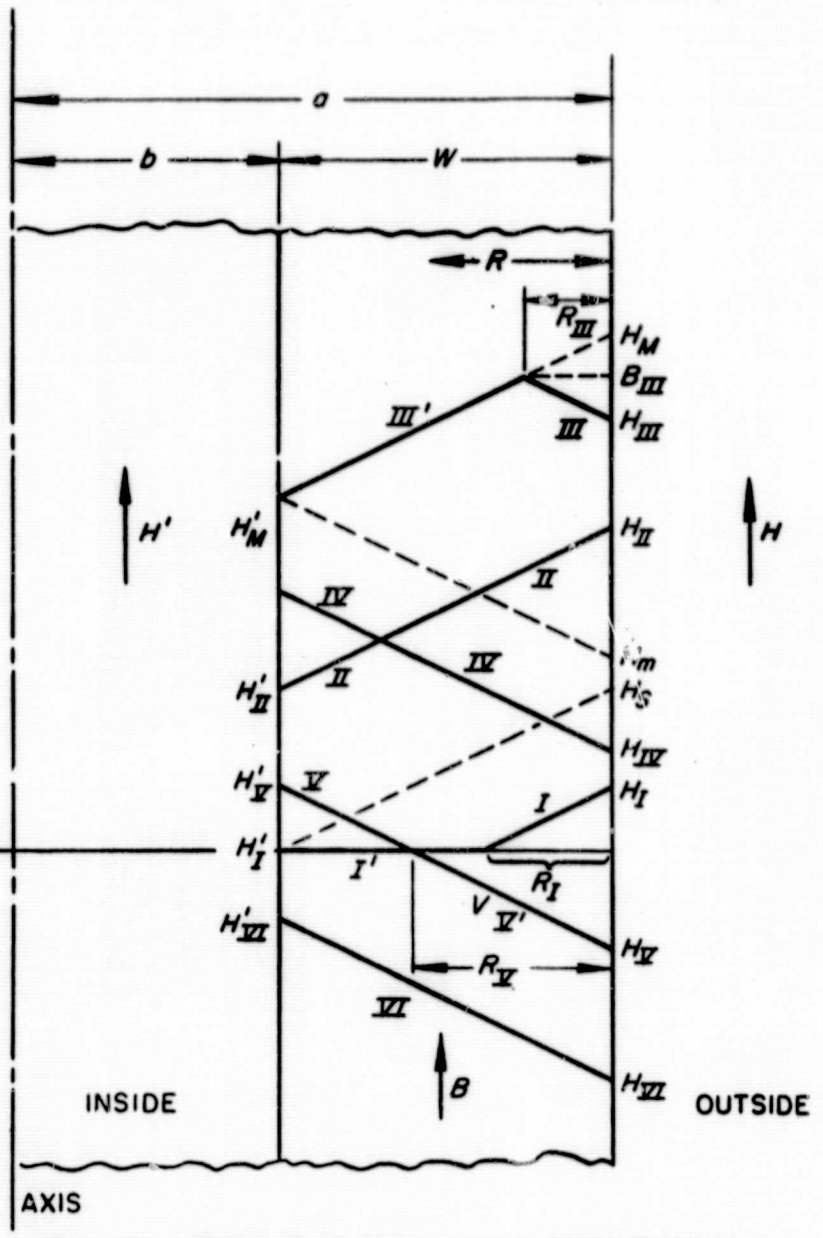

Fig. 2. Field Distribution in a High-Field Superconductor Tube for Different States of a Magnetization Cycle.

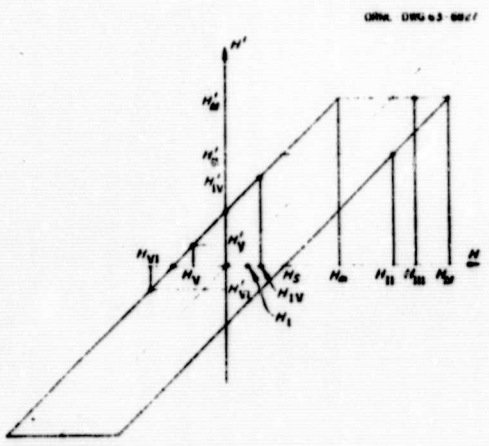

Fig. 3. Tube Magnetization Curve for H. London's Model.

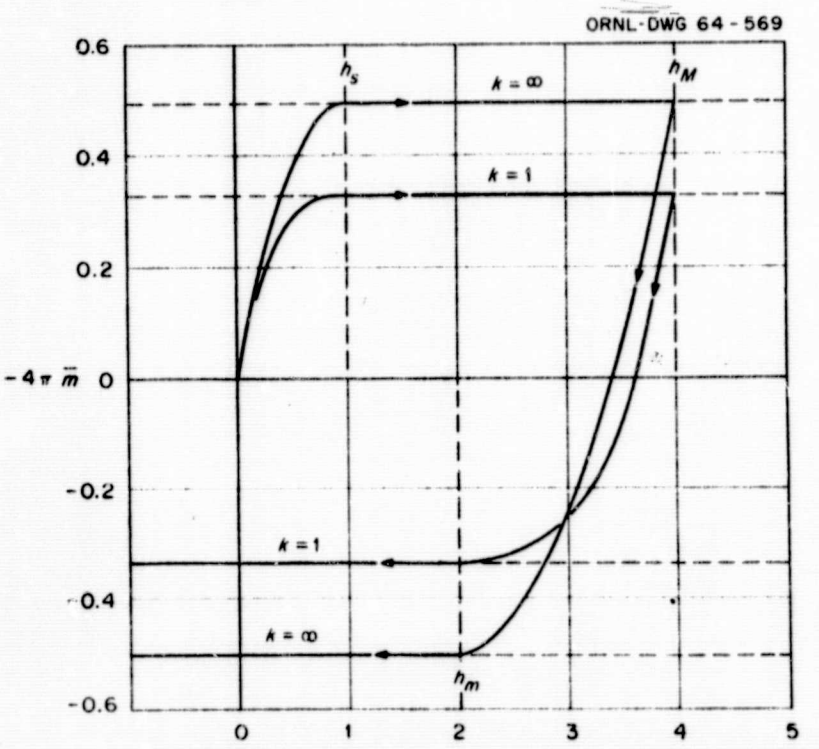

Fig. 4. Magnetic Moment Curves for H. London's Model.

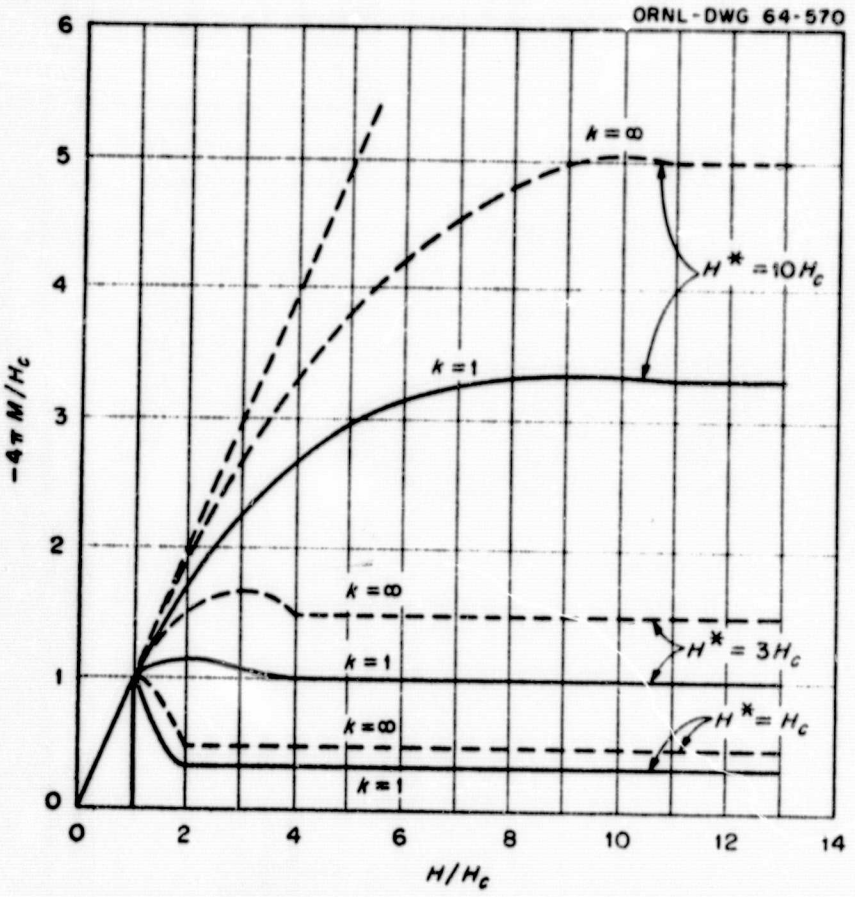

Fig. 5. Magnetic Moment Curves for C. P. Bean's Model.

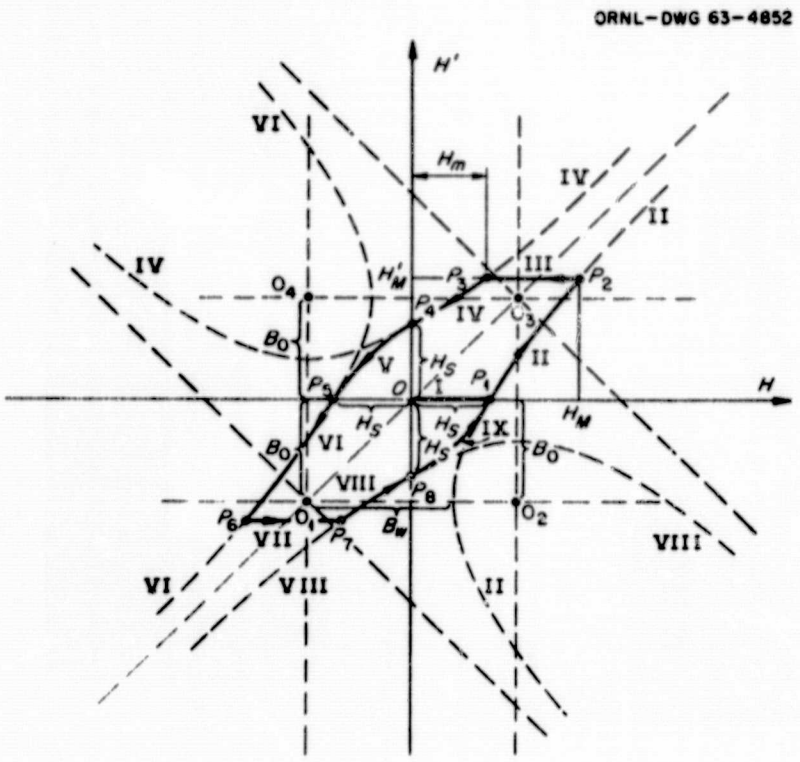

Fig. 6. Tube Magnetization Curves for the Model of Y. B. Kim *et al.*

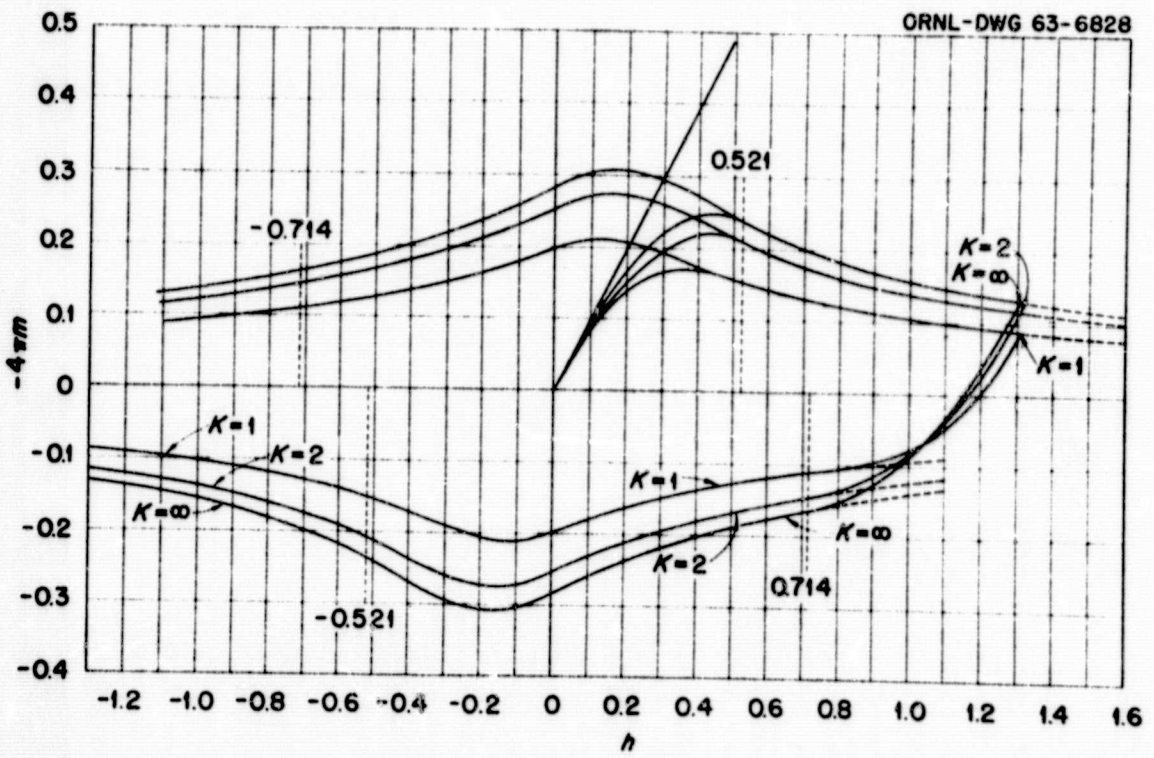

Fig. 7. Magnetic Moment Curve for $b_0 = B_0/H^* = 0.7$ (Model of Y. B. Kim *et al.*).

APPENDIX B

FLUX JUMPS IN COLD-WORKED Nb-25% Zr SOLID AND HOLLOW CYLINDERS UNDER ADIABATIC CONDITIONS

I. THE EXPERIMENTAL METHOD

Figure 1 shows the experimental arrangement. The rate of the field sweep of the superconducting coil M which produces the increasing external field was dH_o/dt = 400 Oe/sec. The sudden change of the flux in the sample S during a flux jump was detected by means of a pickup coil wound around the sample. The resulting signal was recorded either by an X-Y recorder or an oscilloscope. A typical diagram obtained by the X-Y recorder is shown in Fig. 2.

One group of experiments was performed in the following way: The temperature of a sample was changed from room temperature to 4.2°K by immersing into liquid He. In this way each sweep was applied to a "virgin" sample (These types of experiments are marked in Fig. 2 by horizontal arrows). Another group of experiments employed samples with a "magnetic history" (marked by crosses). In these cases the field was raised until the first flux jump occurred and then lowered with a very slow rate in order to avoid a flux jump caused by the decreasing field. At H_o = 0 the sample contained trapped flux. After waiting until the sample achieved thermal equilibrium the field was raised until the first flux jump occurred. The results of these experiments represented in Fig. 2 are as follows: A solid cylinder with 3.2 mm OD and a tube with the same OD and 1.6 mm ID produced approximately the same results. With "virgin" samples the critical field strength H_{Fj} was about 5.5 KOe. In samples with "magnetic history" H_{Fj} increased to around 7 KOe. Although the external conditions were the same, a tube with 3.2 mm OD and a hole of 2.4 mm showed a critical field strength of 4.5 KOe ("virgin" sample) and 5 KOe (sample with "magnetic history"), respectively.

II. DISCUSSION OF THE EXPERIMENTAL RESULTS BY MEANS OF SIMPLE MODELS OF HARD SUPERCONDUCTORS

These results can be explained at least qualitatively by applying Bean's model[1] of hard superconductor.

Figure 3 shows the field and current distribution inside a cylinder in a longitudinal field.

When the external field H_o is increased with a rate of change $\frac{dH_o}{dt}$, flux enters the sample. This change of flux will induce an electric field strength around a concentric circle which has its maximum value E on the surface of the cylinder:

$$2\pi RE = -\frac{d\Phi}{dt} \qquad (1)$$

Because E has the same direction as the shielding current density I_c, an energy per unit volume of

$$dW = EI_c\, dt = \frac{I_c}{2\pi R}\, d\Phi \qquad (2)$$

is dissipated. This leads to a temperature rise dT. Under adiabatic conditions

$$\frac{I_c}{2\pi R}\, d\Phi = c\, dT \quad . \qquad (3)$$

In general I_c, Φ, c, and T are correlated in a rather complicated manner and, therefore, it is impossible to solve this equation analytically. Only for the assumption $R\to\infty$, (3) leads to a simple expression for H_{Fj}. In this case Φ is given by

$$\Phi = 2\pi R\, \frac{B_o}{\mu_o I_c} \cdot \frac{B_o}{2} \qquad (B_o = \mu_o H_o)$$

$$\frac{d\Phi}{dt} = \frac{\pi R}{\mu_o I_c}\, 2\, B_o \frac{dB_o}{dt} = 2\pi RE \qquad (3a)$$

$$dW = E\, I_c\, dt = \frac{B_o}{\mu_o}\, dB_o = c\, dT$$

---

[1] Bean's very simple model does not consider the dependence of I_c on B. It is used here as a first approximation (compare ORNL Thermonuclear Div. Semiann. Prog. Rept., ORNL-3564 for period ending Oct. 31, 1963, pp.107-121).

Integrating gives

$$\frac{B_o^2}{2\mu_o} = \int_{T_o}^{T_c} c(T)\, dT \quad . \qquad (4)$$

If the upper limit of the integral is T_c, the critical temperature at the field B_o, H_{Fj} is determined by $\mu_o H_{Fj} = B_o$. Equation (4) holds not only for Bean's model but also for the case $I_c = \frac{\alpha}{B}$ which is a somewhat simplified form of Kim's model. (4) is identical with an equation derived by Wipf and Lubell[2] in a different way. In the cases considered here (Fig. 2) the simple equation (4) cannot be applied because the condition of large radii (compared with the field penetration depth) is not satisfied. However, it is possible to obtain at least a qualitative explanation of the experimental results if the flux distributions inside the samples are considered.

Figure 4 shows the field distribution at a certain external field strength $H_o = \frac{B_o}{\mu_o} < H_{Fj}$ for the four cases shown in Fig. 2. Equation (3) suggests that the power dissipation increases with the finally achieved magnitude of the flux inside the sample. As shown in Fig. 4a and c ("virgin" samples) in the case of a hollow cylinder, the critical value ø will be achieved at a lower external field than in the case of a solid sample. Figure 4b and d indicate that in the case of trapped flux at $H_o = 0$ α higher external field H_o is necessary in order to achieve the critical flux change. There is no difference in H_{Fj} for the solid sample and the cylinder with 1.6 mm hole, because the field does not penetrate far enough to reach the hole.

Finally, it should be mentioned that Wipf and Lubell's derivation does not lead directly to a geometrical dependence (solid and/or hollow cylinders with various radii). The new derivation shown here considers the rate of flux change which is obviously geometrically dependent.

---

[2] S. L. Wipf and M. S. Lubell, Westinghouse Scientific Paper 65-L JO-Lotem-P3, March 5, 1965.

ORNL DWG. 65-6974

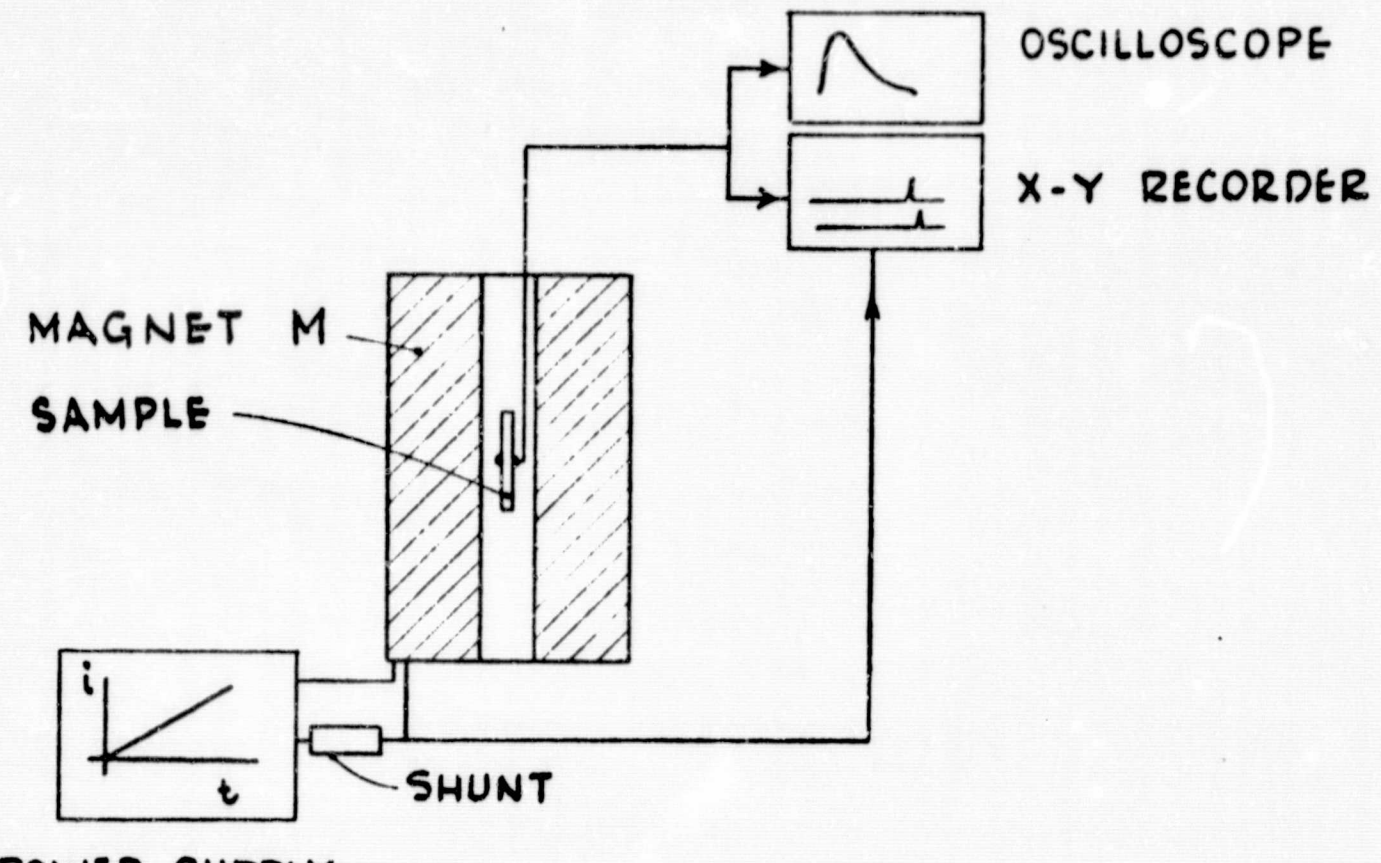

EXPERIMENTAL ARRANGEMENT FOR INVESTIGATION OF FLUX JUMPS IN SUPERCONDUCTING CYLINDERS

Fig 1
App. B

Fig. 2
App. B

ORNL DWG. 65-6975

CRITICAL FIELDS FOR NEARLY ADIABATIC FLUX JUMPS

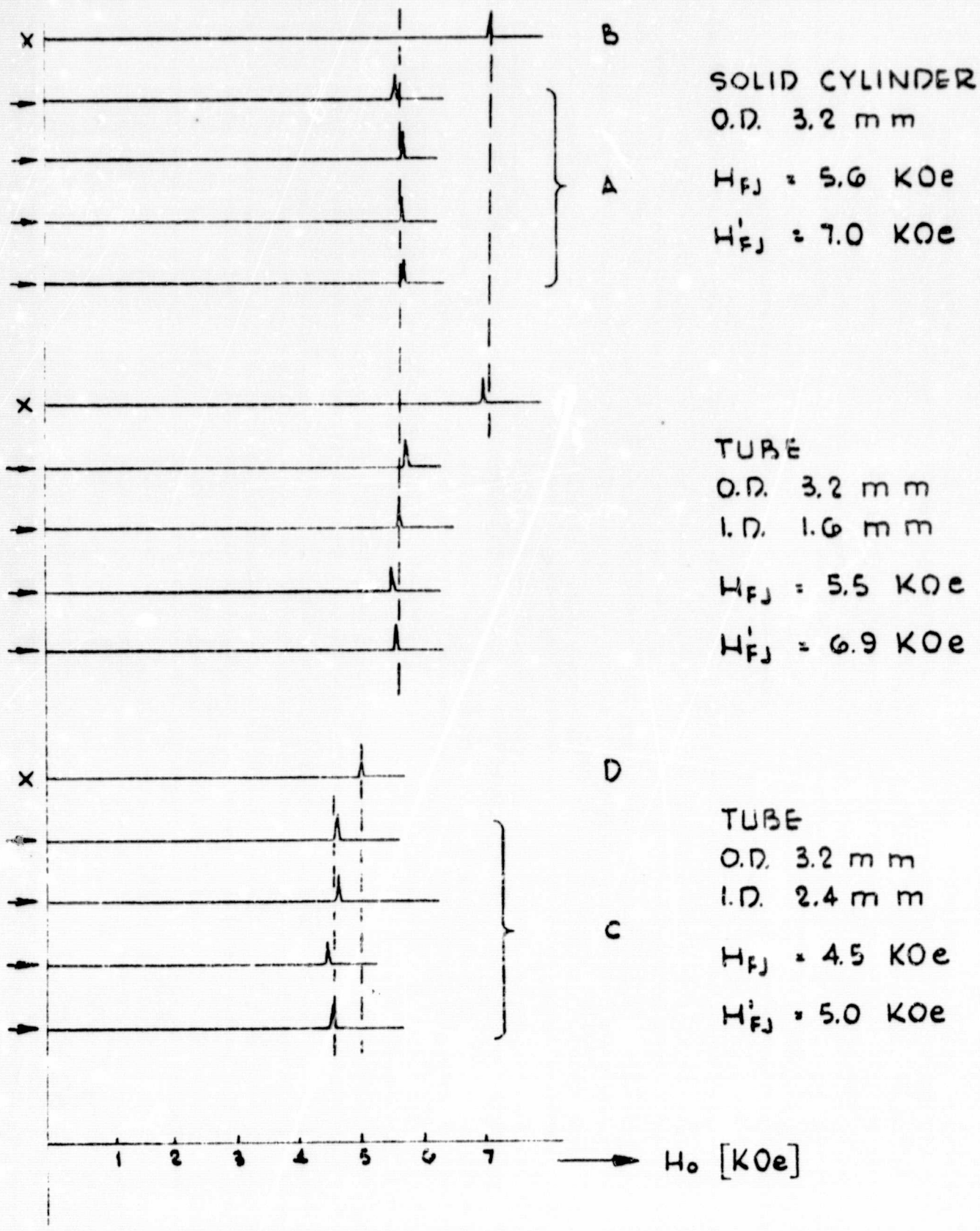

INCREASING FIELDS $\frac{dH_o}{dt}$ = 400 Oe/sec

ORNL DWG. 65-6976

Fig. 3
App. B

FIELD AND SHIELDING CURRENT IN S. C. CYLINDERS

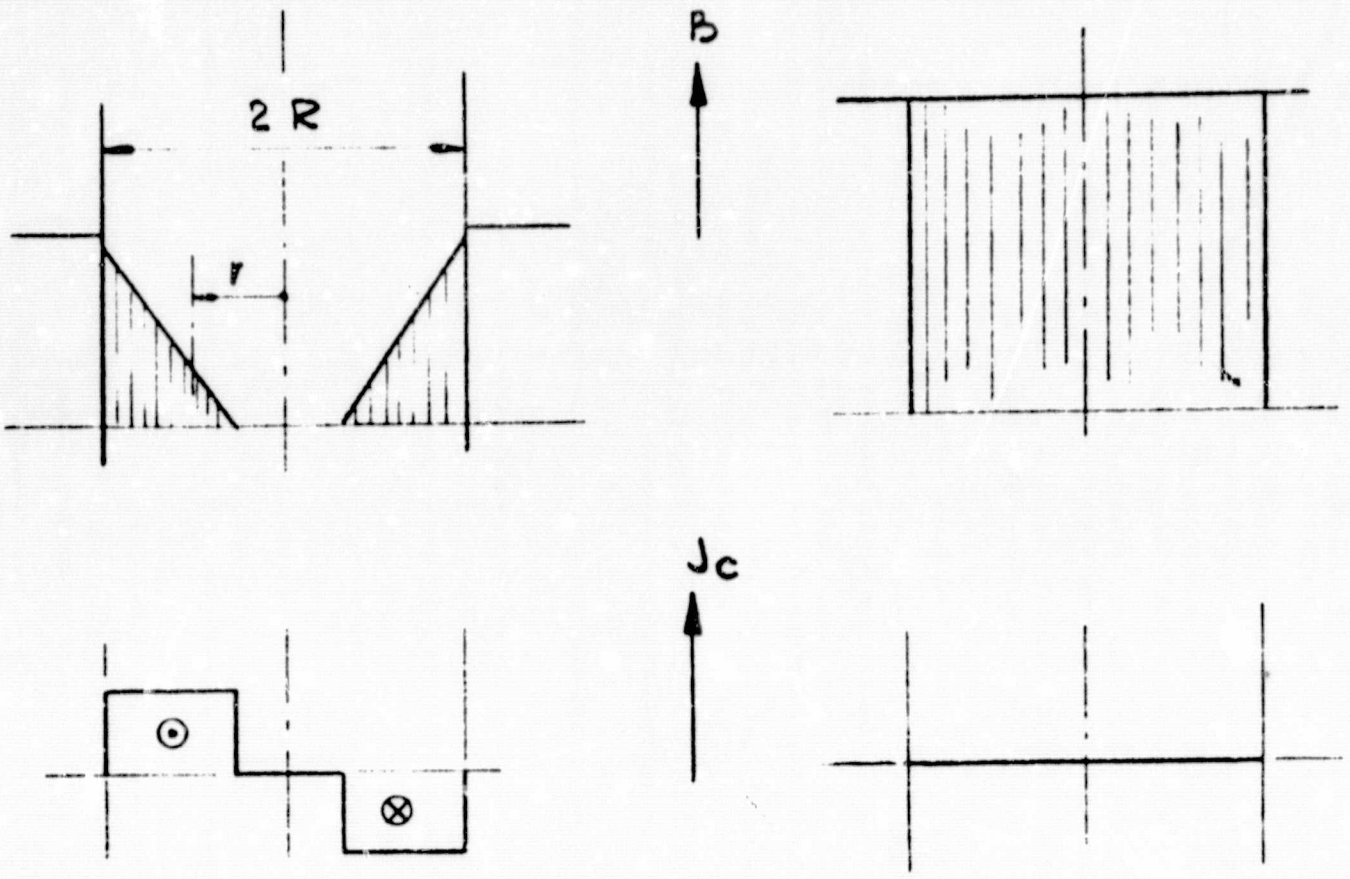

$H < H_{FJ}$
$J_c = J_c(T)$
$T < T_c$

$H > H_{FJ}$
$J_c = 0$
$T > T_c$

ORNL DWG. 65-6977

Fig. 4
App. B

SOLID AND HOLLOW CYLINDERS (WITHOUT AND WITH) TRAPPED FLUX

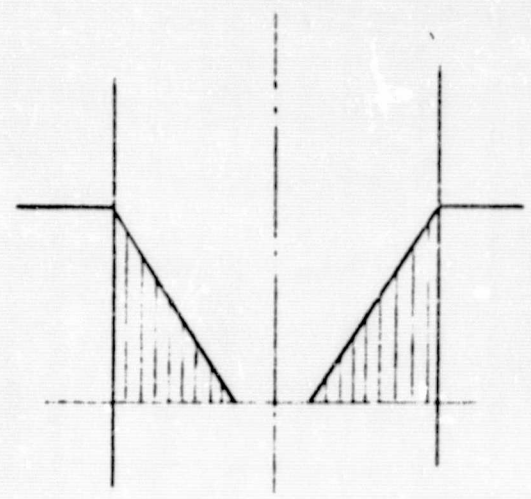

a) SOLID CYLINDER
NO TRAPPED FLUX
AT $H_0 = 0$

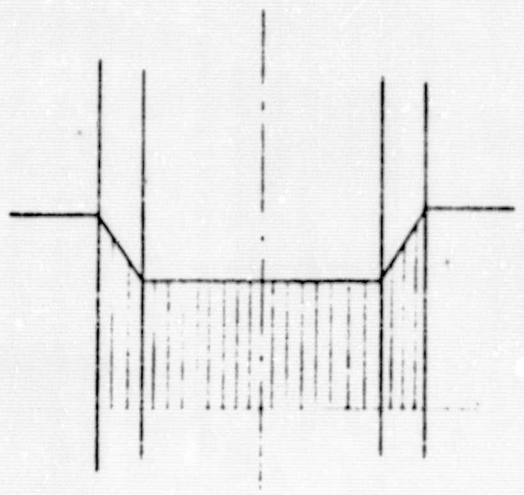

c) HOLLOW CYLINDER
NO TRAPPED FLUX
AT $H_0 = 0$

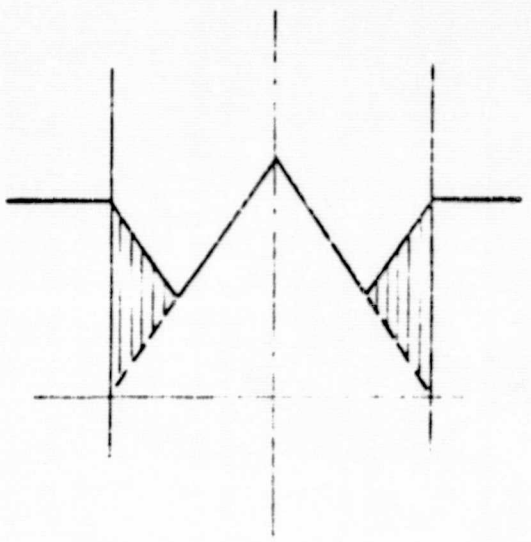

b) SOLID CYLINDER
WITH TRAPPED FLUX

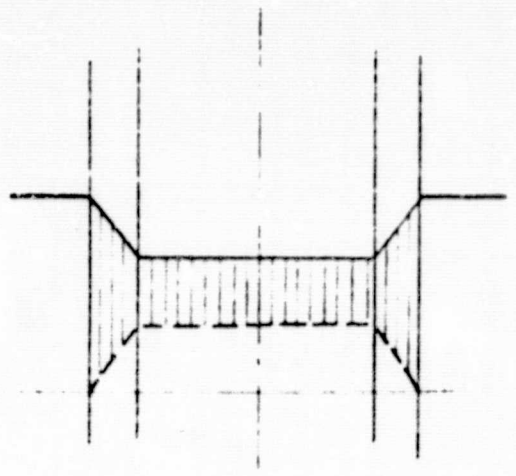

d) HOLLOW CYLINDER
WITH TRAPPED FLUX